Tetrameric UvrD helicase is located at the *E. coli* replisome due to frequent replication blocks

Adam J. M Wollman[1,2,3,], Aisha H. Syeda[1,2], Jamieson A. L. Howard[1,2], Alex Payne-Dwyer[1,2], Andrew Leech[4] , Colin Guy[5, 6], Peter McGlynn[2,6], Michelle Hawkins[2] and Mark C. Leake[1,2]

The authors wish it to be known that, in their opinion, the first two authors should be regarded as joint First Authors

[1] School of Physics, Engineering and Technology, University of York, York YO10 5DD, United Kingdom.

[2] Department of Biology, University of York, York YO10 5DD, United Kingdom.

[3] Current address: Biosciences Institute, Newcastle University, NE1 7RU, United Kingdom.

[4] Bioscience Technology Facility, Department of Biology, University of York, York YO10 5DD, United Kingdom

[5] Current address: Covance Laboratories Ltd., Otley Road, Harrogate, HG3 1PY, United Kingdom

[6] Previous address: School of Medical Sciences, Institute of Medical Sciences, University of Aberdeen, Foresterhill, Aberdeen AB25 2ZD, United Kingdom

* To whom correspondence should be addressed. To whom correspondence should be addressed. Tel: +44 (0)1904322697. Email: mark.leake@york.ac.uk

Present Address: School of Physics, Engineering and Technology, and Department of Biology, University of York, York YO10 5DD, United Kingdom

ABSTRACT

DNA replication in all organisms must overcome nucleoprotein blocks to complete genome duplication. Accessory replicative helicases in *Escherichia coli*, Rep and UvrD, help replication machinery overcome blocks by removing incoming nucleoprotein complexes or aiding the re-initiation of replication. Mechanistic details of Rep function have emerged from recent live cell studies, however, the multiple activities of UvrD in DNA repair and its roles as an accessory helicase in live cells remain unclear. Here, by integrating super-resolved single-molecule fluorescence microscopy with biochemical analysis, we find that UvrD self-associates into a tetramer and, unlike Rep, is not recruited to a specific replisome protein despite being found at approximately 80% of replication forks. Instead, its recruitment to forks is likely mediated by the very high frequency of replication blocks due to DNA bound proteins, including RNA polymerase and DNA damage. Deleting *rep* and DNA repair factor genes *mutS* and *uvrA*, and inhibiting transcription through RNA polymerase

mutation and antibiotic inhibition, indicates that the level of UvrD at the fork is dependent on its function. Our findings show that UvrD is recruited to sites of nucleoprotein blocks via distinctly different mechanisms to Rep and plays a multi-faceted role in ensuring successful DNA replication.

INTRODUCTION

Replication and transcription of DNA occur simultaneously in *Escherichia coli,* making conflicts between the bacterial replisome, the molecular replication machine comprising in excess of 10 different proteins, and RNA polymerase (RNAP) inevitable (1–4). Collisions between the replication and transcription machineries hinder replication fork progression and cause genome instability (5–14). RNAP can pause, stall and backtrack while actively transcribing, and any immobile RNAP molecules present long-lived barriers to replisomes (15, 16). These factors make RNAP the most common nucleoprotein obstacle for translocating replisomes. DNA is also frequently damaged in normal growth conditions due to exposure to endogenous and exogenous DNA damaging agents. The resulting DNA damage also presents significant obstacles for normal replication (17–19).

Several mechanisms exist to reduce conflict between the replisome and obstacles such as transcribing RNAPs. For example, transcription elongation and termination factors reduce the number of immobile RNA polymerases on DNA (1, 18, 20–24). Head-on collisions were originally thought to be more harmful (25–27) and therefore more important to resolve; a view supported by the occurrence of highly transcribed genes encoded on the leading strand, presumably to ensure co-directional transcription and replication (26, 28, 29). However, co-directional collisions of the replisome and transcription machinery also impact replication fork progression (3, 18, 30).

Accessory replicative helicases promote fork movement through nucleoprotein barriers and have been identified in prokaryotes and eukaryotes (1, 12, 13, 31, 32). The Rep and UvrD accessory helicases in *E. coli*, as well as the Pif1 helicase in *Saccharomyces cerevisiae*, perform important roles in helping to clear nucleoprotein complexes (33). More recently, Pif1 has been proposed to be a general displacement helicase for replication bypass of protein blocks, a function similar to the Rep and UvrD helicases (34). These helicases can reduce replisome pausing at several types of

70 native transcription complexes observed in living cells (13, 22, 35), and several types
71 of engineered nucleoprotein blocks in biochemical experiments *in vitro* (1, 31).
72 Rep is the primary accessory helicase in *E. coli*, however, UvrD can partially
73 compensate for the absence of Rep *in vivo* and has been shown to promote replication
74 through stalled transcription elongation complexes (1, 12, 13, 36, 37). UvrD is a
75 superfamily 1 helicase that translocates 3'-5' along ssDNA. The ability of UvrD to
76 compensate partially for the absence of Rep has been attributed to the high degree of
77 homology between these two helicases and the abundance of UvrD inside cells (12,
78 21, 38–40). The role of UvrD in nucleotide excision repair along with UvrABC proteins
79 as well as in methyl-directed mismatch repair along with the MutHLS proteins is well
80 characterised (41–46). UvrD interacts directly with RNAP but the functional
81 importance of this interaction has been unclear until recently (47–50). UvrD has been
82 suggested to promote backtracking of stalled RNAP as a first step in transcription-
83 coupled repair (50, 51); however, other studies argue against UvrD playing any role in
84 coupling nucleotide excision repair to stalled transcription complexes (48, 49, 52–56).
85 Here, we combined state-of-the-art live cell imaging using single-molecule
86 microscopy with advanced biochemical activity experiments *in vitro* to elucidate how
87 UvrD resolves replicative blocks. We used super-resolved high-speed single-molecule
88 fluorescence microscopy of mGFP-UvrD in live cells co-expressing a fork marker,
89 DnaQ-mCherry, to reveal that 80% of DnaQ foci colocalise with UvrD. Stepwise
90 photobleaching intensity analysis showed that UvrD is a tetramer *in vivo*, to be
91 compared with earlier observations performed *in vitro* using analytical
92 ultracentrifugation that found a mixture of UvrD dimers and tetramers (57). Surface
93 plasmon resonance (SPR) measurements of UvrD in combination with each replisome
94 component identified no specific replisome protein interaction partner that would
95 explain replisome-UvrD colocalisation. Deletion of Rep, mismatch repair protein MutS
96 and nucleotide excision repair protein UvrA, and disruption of transcription using either
97 mutation of RNAP or antibiotic inhibition, significantly reduces the number of UvrD or
98 level of observed colocalisation of UvrD with the fork. Coupled with *in vitro* block-
99 dependent differences in UvrD replication promotion efficiency, we conclude that UvrD
100 is located at the *E. coli* replisome due to its role in resolving frequent blocks to
101 replication.
102
103

RESULTS

UvrD is present at the majority of replication forks

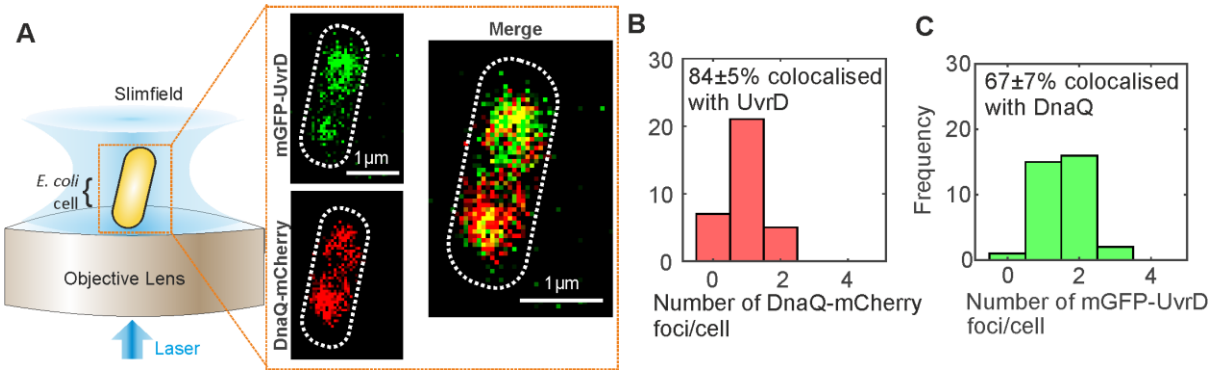

Figure 1: Super-resolved single-molecule light microscopy. (A). Slimfield microscope schematic and Slimfield micrographs of mGFP-UvrD, DnaQ-mCherry. (B) and (C) Histogram showing the number of DnaQ and UvrD foci detected per cell respectively, SD errors.

We investigated the role of UvrD in DNA replication using super-resolved single-molecule fluorescence microscopy to track dynamic patterns of fluorescently labelled UvrD localization relative to the replication fork in live cells (Figure 1A). We performed dual-colour Slimfield (63, 78) to assess the degree of colocalisation between UvrD and the replisome, using a similar imaging protocol as previously for Rep (13). We employed DnaQ-mCherry as a fork marker (13) along with a genomically integrated mGFP-UvrD fluorescent protein fusion construct to report on the localization of UvrD. DnaQ encodes the epsilon subunit, a core component of the DNA polymerase and is well established as a marker for the replication fork (13, 69, 79–81). These strains phenocopied the wild type strain for growth and in plasmid loss assays testing for mGFP-UvrD function retention (Supplementary Figures S1, S2, Tables S1-4). The helicase activity of mGFP-UvrD was comparable to the wild type enzyme in an *in vitro* unwinding assay (Supplementary Figure S3). Under Slimfield, we observed 1-2 DnaQ foci as in the previous study for Rep, corresponding to the two moving replication forks which appear as single foci near the start of replication when they are separated by less than the 200-300 nm diffraction limit of our microscope (Figure 1A,B Supplementary Figure S4). We also observed 1-2 UvrD foci per cell, of which 67 ± 7% (±SEM) were colocalised with DnaQ foci and 84 ± 5% of DnaQ foci were colocalised with UvrD (Figure 1B and C). We calculated the probability of random overlap between these foci, by modelling the nearest-neighbour foci separation as a Poisson distribution (70), to be 20%. To confirm that colocalisation between DnaQ and UvrD was not just a function of the nucleoid association of UvrD, we performed Slimfield

133 imaging of Heat-stable nucleoid-structuring protein (H-NS) tagged with GFP dual
134 labelled with DnaQ-mCherry. H-NS associates with the nucleoid but not specifically
135 with the fork. We found similar numbers of H-NS foci (Supplementary Figure S5) but
136 only 38±4% DnaQ foci were colocalised with H-NS implying that, similarly to the Rep
137 helicase (13), UvrD is present at the majority of replication forks.
138
139 **UvrD is a tetramer in live bacterial cells**
140

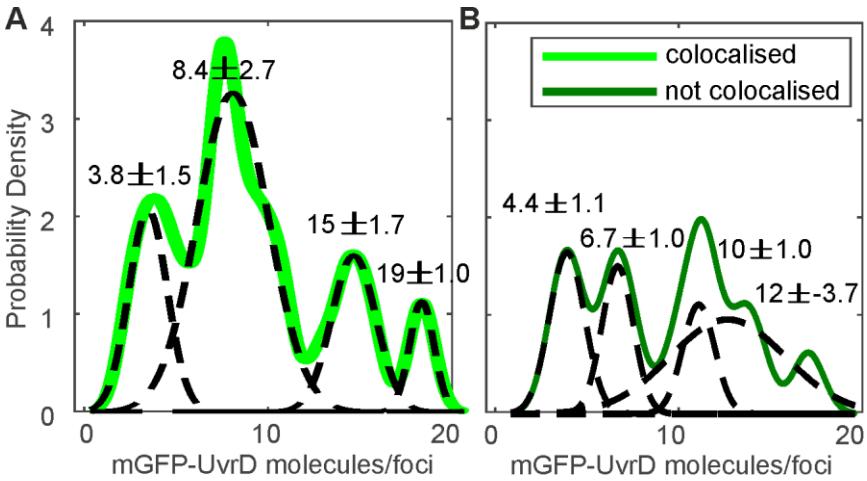

141
142 **Figure 2 UvrD stoichiometry.** The distribution of UvrD foci stoichiometry rendered as a
143 kernel density estimate for foci colocalised (A) and not colocalised (B) with DnaQ foci.
144 Distributions were fitted with multiple Gaussian peaks (black dotted lines) with the peak value
145 ± error determined by the half width at half maximum indicated above each peak
146
147 Slimfield also enabled the stoichiometry of these foci to be determined by utilizing a
148 method involving step-wise photobleaching analysis (69). Here, we determined the
149 brightness of a single-molecule of mGFP or mCherry fluorescent protein under our
150 Slimfield imaging conditions (Supplementary Figure S7), and used these values to
151 normalize the initial brightness of all tracked foci as an estimate for the apparent
152 stoichiometry in terms of number of fluorescently labelled molecules present. We
153 found that DnaQ had the same range of 2-6 molecules per focus (Supplementary
154 Figure S8) as we have found previously, corresponding to 2-3 polymerases per fork
155 (13, 69). The distribution of the apparent stoichiometry of UvrD foci which are
156 colocalised with DnaQ had a distinct lowest-order peak corresponding to
157 approximately four molecules, with subsequent peaks at clear multiples of four (Figure
158 2A). UvrD foci that are not colocalised with DnaQ also contained a distinct lowest-
159 order peak at four, but subsequent peaks were less clearly tetrameric. We performed

160 Size Exclusion Chromatography - Multi-Angle Laser Light Scattering (SEC-MALLS) to
161 test whether the fluorescent protein labelling UvrD might be inducing multimers but
162 found limited effects on UvrD assembly state, as expected from the K_D dissociation
163 constant of fluorescent proteins containing the A206K mutation (82) (Supplementary
164 Figure S9). UvrD has been shown to exist in a monomer-dimer-tetramer equilibrium
165 *in vitro* (57). DNA unwinding experiments *in vitro* suggest UvrD must function as at
166 least a dimer (83) or a trimer (84), however the oligomeric state of functional UvrD is
167 disputed (reviewed in (85)). To our knowledge, these are the first UvrD stoichiometry
168 measurements *in vivo* so we propose that UvrD forms a tetramer *in vivo* with multiple
169 tetramers often at the replication fork. It should be noted that we often observe only a
170 single DnaQ focus corresponding to two replication forks which are separated by less
171 than the diffraction limit of our microscope (Supplementary Figure S8) such that some
172 multiple tetramer UvrD foci correspond to two replication forks. The less distinct peaks
173 in the UvrD foci that are not colocalised with DnaQ may indicate that other UvrD
174 species (monomers, dimers or trimers) are also present.
175 We were also able to determine the total cell copy number of UvrD using a
176 method which determined the total contribution of mGFP-UvrD fluorescence to the
177 observed intensity in whole cells (72). We found approximately 800 molecules of UvrD
178 per cell (Supplementary Figure S10), similar to that which we reported previously for
179 Rep (13). This is a much lower level of UvrD than was reported using transcription rate
180 measurements (86) or high-throughput proteomics (87) but is comparable to recent
181 estimates using ribosome profiling (88).
182
183 **No interaction partner was found for UvrD at the fork with SPR**
184 Our earlier findings concerning the accessory helicase Rep indicated that
185 colocalisation with the fork and recruitment to the replisome were mediated by specific
186 interaction with the replicative helicase DnaB (89), with Rep and DnaB both exhibiting
187 hexameric stoichiometry (13, 69). We sought to determine whether UvrD is also
188 recruited by interacting with a specific replisome component using SPR on purified
189 UvrD and each replisome component (Supplementary Figure 11). UvrD exhibited no
190 direct interaction with primase, SSB, β sliding clamp, the DNA polymerase III αε, χψ
191 or γ complexes; or θ, δ, δ′, χ, and γ subunits (12). We did initially identify a putative
192 weak UvrD-Tau interaction. However, as a control we also tested Rep, and found this
193 also interacted with Tau to a similar extent, and with ~100x lower affinity than UvrD

194 with known interaction partner UvrB (Supplementary Figure 8). We therefore conclude
195 that the Tau interaction with UvrD is non-specific and that, unlike Rep, UvrD likely does
196 not have a direct interaction partner at the replisome from the suite of replisome
197 proteins tested. As UvrD is a tetramer at the replisome, it is also unlikely to be recruited
198 by Rep, which has shown putative interaction (90).
199

200 **UvrD presence at the replication fork is mediated by specific blocks to**
201 **replication**

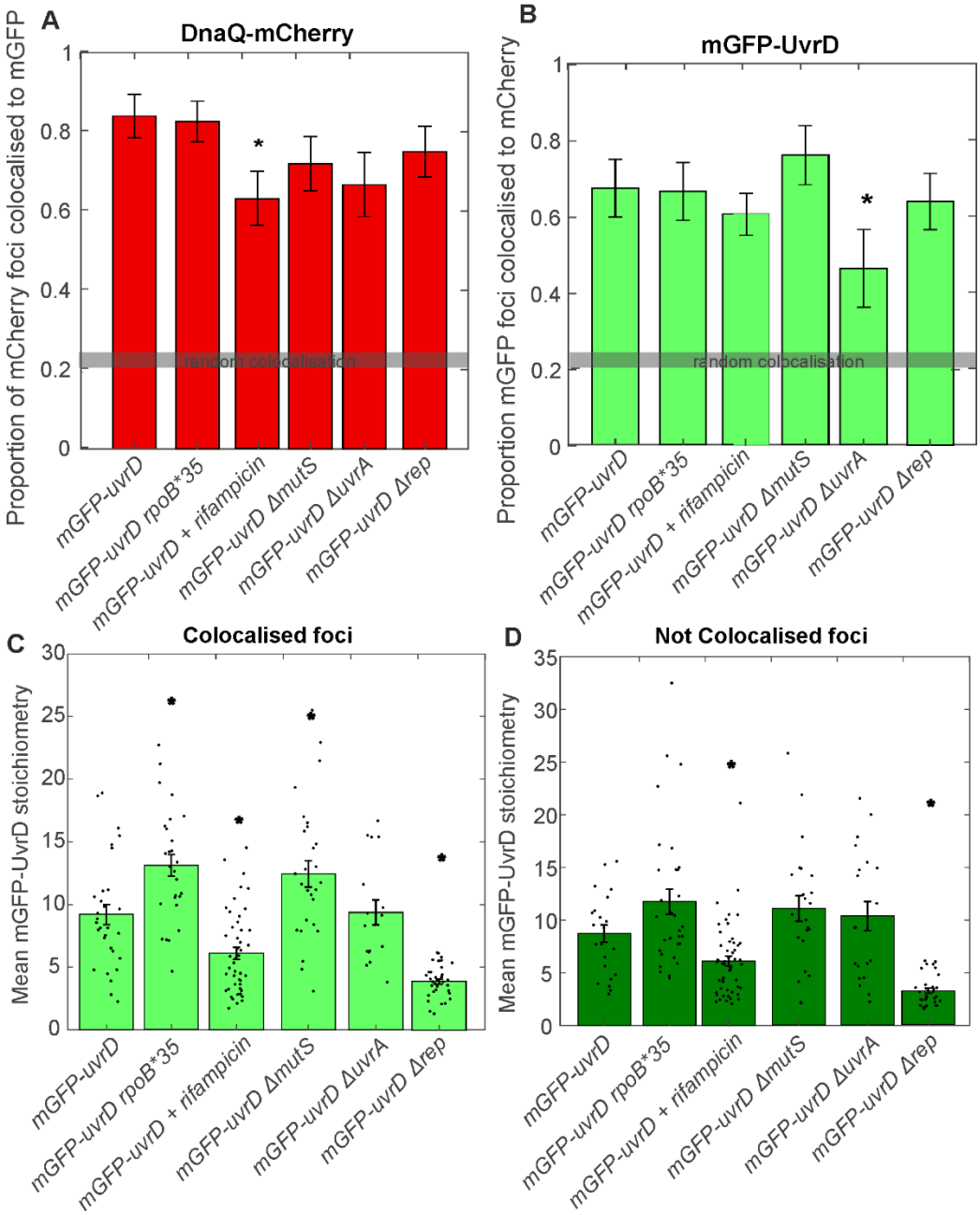

202

203 **Figure 3: UvrD perturbations.** A. and B. The mean proportion of colocalised DnaQ and UvrD
204 foci per cell respectively. Error bars represent standard error in the mean and statistical

205 significance by Student's t-test $p<0.05$ indicated by *. C. and D. Jitter plots of colocalised and
206 not colocalised UvrD stoichiometry respectively. Bars show mean UvrD stoichiometry with
207 error bars showing the standard error in the mean and statistical significance by Student's t-
208 tests $p<0.05$ indicated by *.
209
210 Since our SPR observations indicated that UvrD does not interact directly and
211 specifically with any core replisome protein, we hypothesized that the association of
212 UvrD with the replication fork might be dependent on its activity in resolving
213 nucleoprotein blocks. To test this, we systematically impaired key DNA replication
214 repair processes in which UvrD is implicated, as well as perturbing RNAP replicative
215 blocks by disruption of transcription through both genetic mutation and antibiotic
216 inhibition (Figure 3). We perturbed UvrD's activity in resolving DNA damage at
217 replication blocks by deleting *mutS* or *uvrA*, rendering the strains defective in UvrD-
218 associated mismatch repair or nucleotide excision repair respectively (43, 91). We
219 reduced the need for UvrD to remove transcriptional blocks to replication (49) by
220 introducing the *rpoB*35* mutation, which destabilizes open complexes formed during
221 initiation of transcription (92, 93); and by using the antibiotic rifampicin, which blocks
222 elongation of RNA transcripts (94). All of these strains were healthy under normal
223 growth conditions (Supplementary Figure S1, Table S4) and displayed the same
224 phenotype for DnaQ foci number and stoichiometry within measurement error
225 (Supplementary Figure S8).
226 For the transcriptional block perturbations, the *rpoB*35* mutant dual labelled
227 strain exhibited no difference in the proportion of colocalised DnaQ or UvrD foci
228 (Figure 3A and B). This mutant and all others tested exhibited the same predominant
229 tetrameric stoichiometry trends as wild type (Supplementary Figure S12), with clear
230 peaks at tetramer intervals in the colocalised stoichiometry distribution and less clear
231 but still largely tetrameric intervals in the stoichiometry distribution for UvrD foci that
232 are not colocalised with DnaQ. This provides further evidence that UvrD operates
233 predominantly as a tetramer *in vivo*. We compared the mean stoichiometry for each
234 mutant to that of wild type (Figure 3C and D). Unexpectedly, the *rpoB*35* mutant
235 produced a slight but statistically significant increase in mean colocalised
236 stoichiometry, corresponding to approximately one extra UvrD tetramer at the
237 replication fork (Figure 3C). This finding may indicate the level of instability conferred
238 by this mutation has multiple downstream effects that alter UvrD localisation
239 significantly at the fork. Alternatively, it could mean that *rpoB*35* does not affect the

240 formation of the types of transcriptional block that are acted upon by UvrD. Rifampicin
241 treatment produced a clearer response, reducing the number of DnaQ foci colocalised
242 with UvrD by ~20% (Figure 3A) and the mean stoichiometry of colocalised and not
243 colocalised UvrD foci by around one UvrD tetramer (Figure 3C and D). Single-
244 molecule observations of RNAP have shown it to be significantly more mobile under
245 rifampicin treatment (95), implying fewer RNAPs bound to DNA and fewer blocks to
246 replication. Our rifampicin treatment results are consistent with fewer transcriptional
247 blocks to replication reducing the amount of UvrD recruited to the replisome and
248 support the hypothesis that UvrD is recruited by these replicative blocks.
249 By deleting *mutS* or *uvrA* we removed UvrD's role in mismatch repair and
250 nucleotide excision repair respectively. Deleting *mutS* surprisingly resulted in no
251 change in UvrD colocalisation with DnaQ but did increase the mean UvrD
252 stoichiometry colocalised with DnaQ by around one tetramer (Figure 3A). In the Δ*uvrA*
253 mutant this resulted in a clear drop of ~25% in UvrD colocalisation with DnaQ (Figure
254 3B) with no change in the number of UvrD foci (Supplementary Figure S8), consistent
255 with the hypothesis that UvrD association with the fork is dependent on actively
256 resolving DNA damage induced blocks to replication. The minimal response in the
257 Δ*mutS* strain may also suggest that UvrD at the fork is more involved in nucleotide
258 excision repair than mismatch repair.
259 UvrD has been shown to compensate for Rep in *rep* null mutants (12). We also
260 tested what effect this mutation would have in our single-molecule assay. Surprisingly,
261 *rep* deletion resulted in a steep drop in UvrD copy number (Supplementary Figure
262 S10). The degree of colocalisation between UvrD and DnaQ remained unchanged
263 compared to wild type (Figure 3A and B) but the stoichiometry of foci was reduced to
264 a single UvrD tetramer (Figure 3C and D and Supplementary Figure 11), presumably
265 due to the lower copy number and availability of UvrD. The drop in UvrD copy number
266 may reflect complex regulatory shifts in response to losing such a key protein in Rep,
267 although it is interesting that even at low copy numbers, a UvrD tetramer remains
268 recruited to the fork. Double knockouts, deficient in both Rep and UvrD, are lethal (12)
269 so this minimal helicase presence must be the limit required for survival.
270

The dynamic association of UvrD with the replication fork is dependent on repair processing

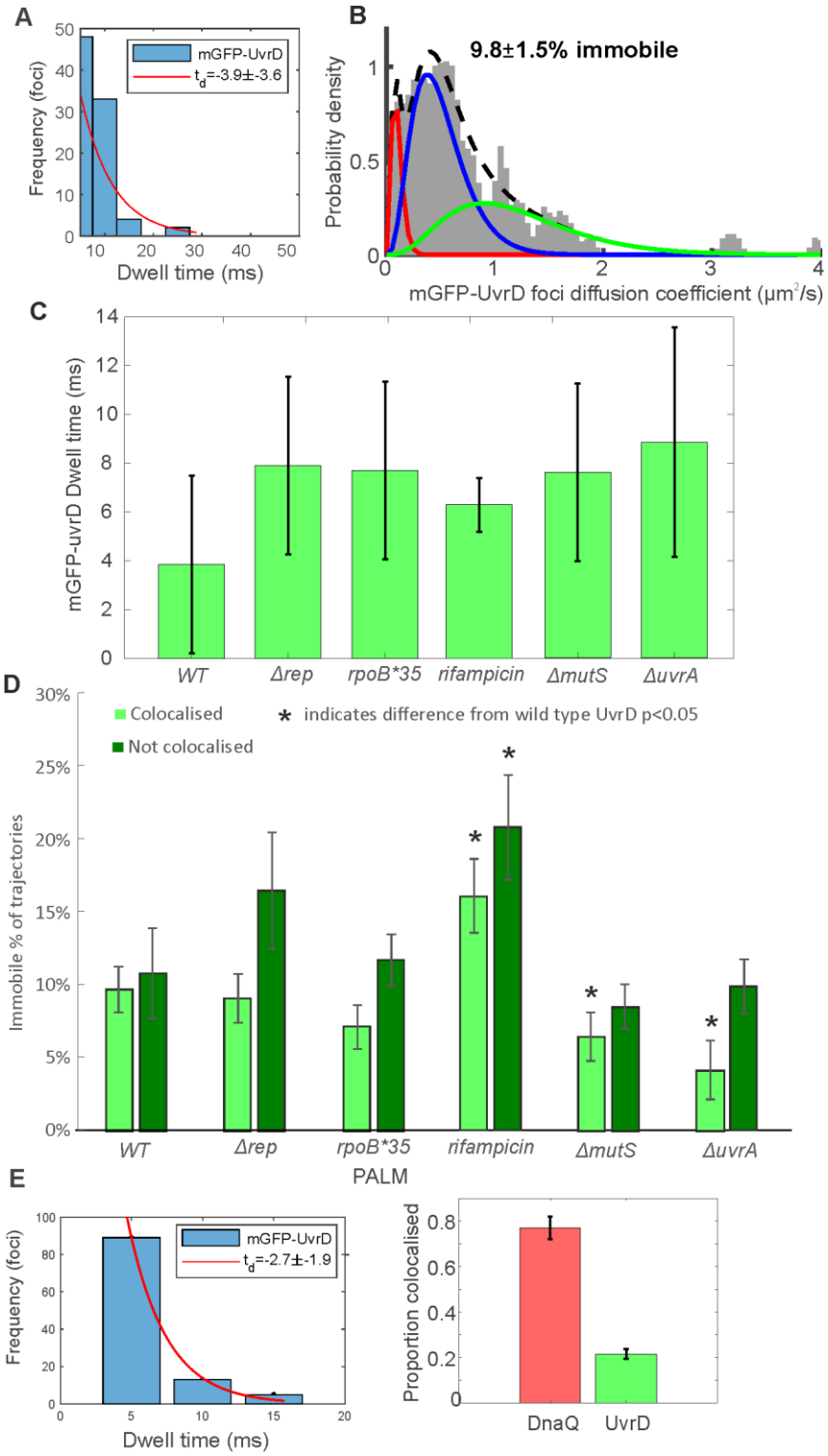

Figure 4: UvrD dynamics. A. Distribution of time over which UvrD and DnaQ foci were colocalised (blue) fitted with an exponential (red) to yield a characteristic dwell time. B. Distribution of microscopic diffusion coefficients of wild type UvrD foci (grey) fitted with a three state gamma distribution model containing a relatively immobile population with $D = 0.1$ $\mu m^2/s$ (red), a transiently immobile population, $D = 0.5$ $\mu m^2/s$ (blue) and a mobile population,

D=1.2 μm^2/s (green). C. The dwell times for each UvrD strain. Error bars represent the 95% confidence intervals on the fit. D. The proportion of UvrD foci in the immobile population for each UvrD strain colocalised or not colocalised with DnaQ foci location. Statistically significant differences $p<0.05$ from wild type indicated by *. E. PALM dwell time and colocalisation proportion of detected tracks.

By tracking UvrD foci as a function of time using rapid millisecond timescale sampling in Slimfield imaging, we were also able to characterize its dynamics in wild type and repair impaired cells. We measured the number of frames UvrD foci were colocalised with DnaQ foci positions, the dwell time, and calculated the apparent microscopic diffusion coefficient of individual foci (Figure 4 and Supplementary Figure S13). The UvrD dwell time at the fork for the wild type strain was measured to be approximately 4 ms, indicating a relatively dynamic association of UvrD at the replication fork. The apparent microscopic diffusion coefficients (*D*) were best fit with a three parameter Gamma model, containing a relatively immobile population with $D = 0.1$ μm^2/s, a transiently immobile population, $D = 0.5$ μm^2/s and a mobile population, D=1.2 μm^2/s, similar to Rep (13). In wild type, we found approximately 10% of UvrD foci were immobile, whether colocalised with the DnaQ fork location or not, with the rest of the foci split between the other two populations.

We sought to use these molecular measurements to determine the effect of perturbing UvrD-mediated DNA replication repair and block resolution on UvrD dynamics. All deletions resulted in a marginal though statistically negligible increase in dwell time to between 6-9 ms. The Δ*rep* and *rpoB*35* mutations resulted in no change in mobility from wild type. Rifampicin treatment however, resulted in an increase in the proportion of immobile foci both at and away from the fork. This finding appears counterintuitive as rifampicin treatment results in more mobile RNAP (95), however it is unclear what effect rifampicin has on the population of RNAP molecules that remain bound to DNA. These results may suggest that such blocks provide an increased barrier to replication, decreasing mobility of UvrD as it attempts to deal with these blocks. In the Δ*mutS* and Δ*uvrA* strains, the proportion of immobile foci decreased at the fork, again consistent with the hypothesis that UvrD association with the fork is dependent on DNA damage resolution activity. An alternative explanation for these results is that UvrD is less mobile when resolving DNA damage blocks to replication and more mobile when resolving transcriptional blocks, as reducing or

313 eliminating UvrD's role in these processes decreased or increased the immobile
314 fraction in DNA repair and transcription impaired cells respectively (Figure 4).
315
316 ***In vitro* experiments confirm block-dependent UvrD function**
317 To further investigate the role of blocks in UvrD recruitment to the replisome, we
318 performed a stalled replication assay *in vitro,* which allowed us to specifically vary the
319 nucleoprotein block and the timing of UvrD recruitment i.e. before or after the
320 replisome had encountered the block. *E. coli* replisomes can be reconstituted on
321 plasmid DNA templates containing *oriC* and engineered stall sites. UvrD can be
322 included from the start of replication or added after the replisome has encountered the
323 nucleoprotein block. Blocked fork resolution was then probed by examining replication
324 products by denaturing gel electrophoresis.
325 We first used an *oriC*-containing plasmid which contained a specific RNAP stall
326 site ($P_{lacUV5\ 52C}$) to facilitate formation of a stalled transcription elongation complex via
327 nucleotide deprivation. Stalled RNAP acts as a barrier to the replisome in both head-
328 on and co-directional orientations and prevents the formation of full-length replication
329 products (1). Arresting the replisome at this RNAP block resulted in replication
330 products consisting of four truncated leading strands. The strand sizes matched those
331 expected for replisomes moving clockwise or counter-clockwise from *oriC* and
332 encountering $P_{lacUV5\ 52C}$ or the promoters within the *ColE1* plasmid origin of replication
333 (Figure 5A, lane 2 and Figure 5C) (1).
334 Inclusion of UvrD before replication initiation enabled movement of replisomes
335 through stalled RNAP and resulted in a decrease in all four truncated leading strand
336 products and a concomitant increase in production of full-length leading strands
337 (Figure 5A, lane 5 and 5E) (1). Addition of UvrD once the replisome had already
338 encountered the block gave variable results that ranged from an inhibitory to a stronger
339 effect, although differences were not statistically significant at $p<0.05$ (Figure 5A,
340 compare lane 5 with 6, Figure 5E). Similar results were also obtained for Rep (Figure
341 5A, compare lane 3 with 4, Figure 5E). In the absence of replication neither Rep nor
342 UvrD are capable of pushing stalled RNAP from the $P_{lacUV5\ 52C}$ stall site (1). We found
343 that the mGFP tag does not prevent UvrD from dislodging a protein block
344 (Supplementary Figure S14).

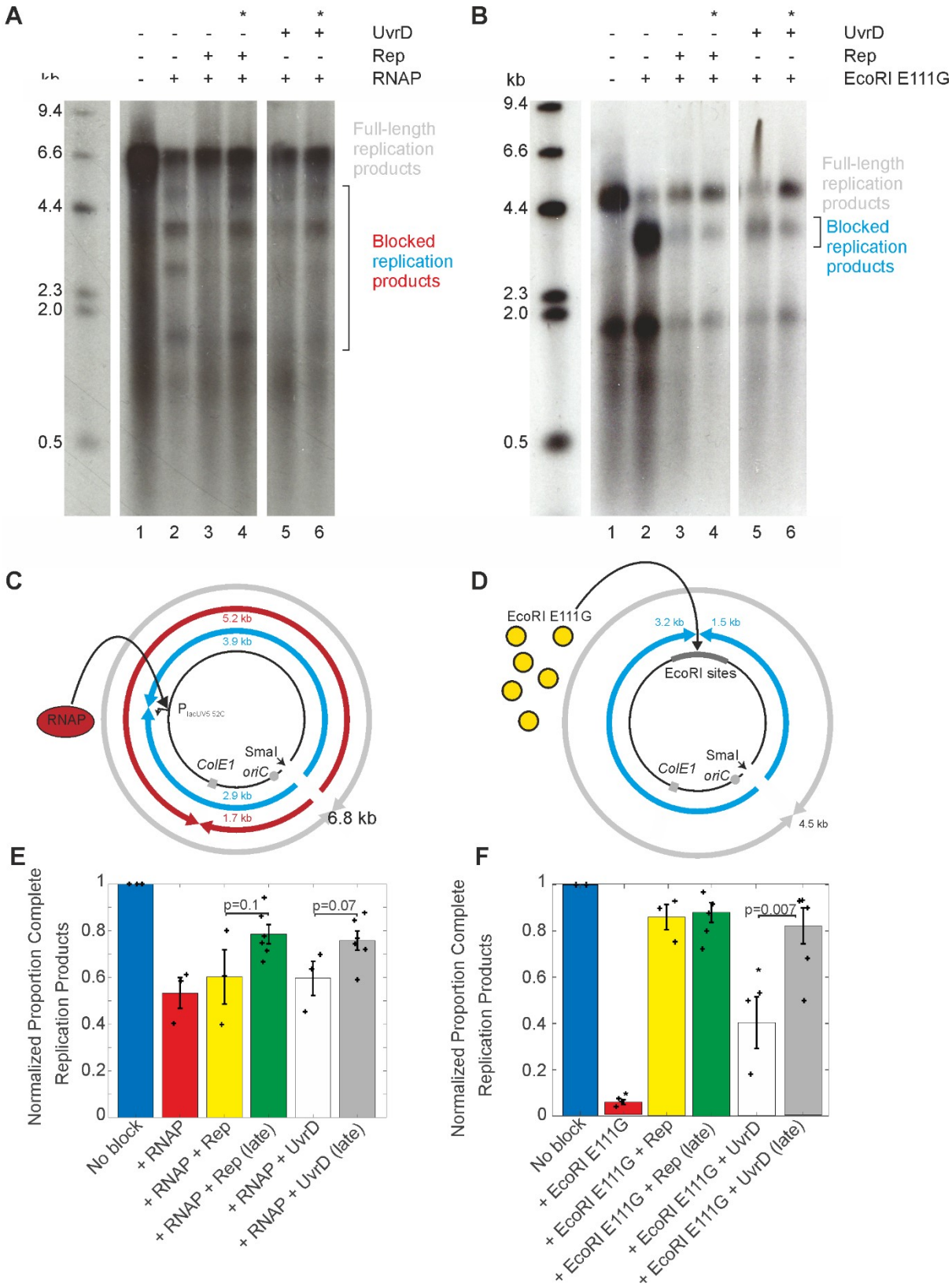

Figure 5: Helicase pre-association affects the promotion of replication fork movement through different nucleoprotein blocks A. Denaturing agarose gel of replication products formed from pPM872 (1) in the absence and presence of RNAP block, Rep and UvrD added pre- and post-collision (*) as indicated. B. Denaturing agarose gel of replication products formed from pPM594 (12) in the absence and presence of EcoRI E111G block, Rep and UvrD added pre- and post-collision (*) as indicated. Truncated leading strand products formed by

352 replisomes originating from *oriC* and colliding with RNAP (C) and EcoRI E111G (D).
353 Quantification of lanes in (A) and (B) from three technical replicates shown in (E) and (F),
354 with standard error in the mean indicated and each replicate result shown as a cross.
355

356 Since UvrD has been shown to interact with RNAP (47–49), we tested whether UvrD-
357 block pre-association is a requirement for its promotion of replication. EcoRI E111G is
358 a mutant restriction enzyme that binds to its recognition sequence but has reduced
359 cleavage activity (96). EcoRI E111G can thus act as an engineered replication fork
360 block that can be overcome by Rep or UvrD helicase activity (12). We tested whether
361 UvrD helicase could promote replication through this barrier when added before or
362 after initiation of replication on a plasmid template with an array of eight EcoRI sites
363 (Figure 5B and D). Adding UvrD post-collision did not impede its promotion of
364 replication; in fact the resolution of these collisions appeared to be more efficient
365 because the proportion of full-length replication products increased (Figure 5B,
366 compare lane 5 and 6, 5F). Quantification of full-length replication products as a
367 proportion of reaction products showed that late UvrD addition increased full-length
368 replication products to 84% (n=6) from 41% (n=3) when UvrD is present before fork
369 collision. This contrasts with the RNAP block results where the UvrD-RNAP interaction
370 (47–50) might be responsible for localising UvrD to the block and facilitating resolution,
371 resulting in no difference when present pre- or post-collision. Similarly, Rep associates
372 directly with the replication fork, also resulting in no difference when present pre- or
373 post-collision, for both blocks. These results suggest that UvrD might recognize stalled
374 replication forks at nucleoprotein blocks using a different mechanism than Rep.
375 Combining these data with the lack of a specific replisome partner and reductions in
376 colocalisation between UvrD and DnaQ fork marker when replication blocks are
377 perturbed *in vivo*, leads us to propose that UvrD is present at the replication fork due
378 to the high frequency of different types of blocks to replication.
379

380 **DISCUSSION**

381 Here, we show that the majority of replisomes are associated with UvrD; but unlike the
382 established Rep association, UvrD has no interaction partner in the replisome. UvrD
383 instead associates with the replisome through the frequent blocks to replication
384 encountered by the fork. Similarly to Rep, *in vitro* evidence suggests UvrD functions
385 poorly as a helicase when monomeric (97). We showed previously that functional Rep
386 foci were hexameric *in vivo* but that this oligomerisation is due to interactions with

387 hexameric DnaB (13). Again, UvrD functions differently and appears to self-associate
388 into tetramers, as evidenced here by tetramer periodicity at and away from the fork
389 (Figure 2 and Supplementary Figure 11) and previous ultracentrifugation experiments
390 *in vitro* (57). It is possible that UvrD may not have evolved to fulfil exactly the same
391 function as Rep. It is common in many enzyme-catalysed reactions that if one enzyme
392 is depleted then another will be available to take its place, but with a reduced catalytic
393 efficiency (98). On initial inspection, this might appear to be the case for Rep and
394 UvrD, in light of the lower efficiency of block resolution for UvrD compared to Rep,
395 noting that deletion of Rep has a profound impact on replication whereas lack of UvrD
396 does not (99). However, we have shown that Rep and UvrD have distinctly different
397 modes of recruitment at a replication block. These differing mechanisms of replication
398 promotion may suggest a model in which these accessory helicases have evolved to
399 fulfil the same overall function (i.e. that of resolving a block to DNA replication) but in
400 different ways. Even with different block removal efficiency, such redundancy may
401 confer an increased level of robustness, helping to ensure that the vital process of
402 DNA replication is carried out correctly by the cell.
403 We used single-molecule microscopy to show that a high proportion of forks,
404 80%, are associated with UvrD *in vivo.* Although the raw imaging data of our Slimfield
405 microscopy is still subject to the optical resolution; the localization tracking algorithms
406 applied can pinpoint fluorescently labelled UvrD to approximately 40 nm lateral
407 precision, smaller than the 50 nm diameter of the replisome machinery itself (69) and
408 equivalent to ~100 bp DNA. Thus, our measurements for colocalisation between UvrD
409 and DnaQ are likely to be good indicators of a real interaction between the replication
410 fork and UvrD. Importantly, the degree of colocalisation we observed is much higher
411 than expectations of random overlap of the optical images of DnaQ-mCherry and
412 mGFP-UvrD.

413 Through SPR, however, we could not find any interaction partner at the
414 replisome apart from Tau. As a control, we tested Tau's interaction with a Rep
415 helicase, and also found a positive interaction. Thus, we conclude that the interaction
416 of UvrD with Tau is likely non-specific and UvrD recruitment to the replisome is
417 mediated by blocks, rather than an interaction partner at the replisome. However, we
418 cannot know the oligomeric state of UvrD on the SPR chip and UvrD's tetrameric form
419 may affect its interactions with replisome components.

420 We probed UvrD's function at the replication fork by perturbing its known DNA
421 repair processing functions, specifically by knocking out *mutS* and *uvrA*, thus blocking
422 mismatch and nucleotide excision repair respectively. We also introduced a mutant
423 RNAP with *rpoB*35* and treated the wild type with rifampicin to reduce the occurrence
424 of transcriptional blocks to translocating replication machinery. Deleting *uvrA* and
425 rifampicin treatment produced clear results, reduced fork colocalization, but deleting
426 *mutS* and introducing the *rpoB*35* mutation did not. However these latter perturbations
427 did result in an identical phenotype of one extra UvrD tetramer per fork. The *rpoB*35*
428 mutation improves cell viability to increased DNA lesions (92). This intriguing link
429 between mutations requires further study, possibly of these dual labelled strains in
430 response to increased DNA lesions. These data support the hypothesis that UvrD is
431 recruited to the replisome by replicative blocks. This is substantiated by the reduced
432 frequency of colocalization observed when mismatch repair and nucleotide excision
433 repair pathways involving UvrD are disrupted. RNA polymerases are the most
434 frequently encountered barrier to replication and we also see a reduction in
435 colocalization when RNA polymerases are removed by the antibiotic.
436 The only function of UvrD we did not probe directly here was its role in RecA-
437 mediated recruitment. We believe the results from a *recA* knockdown would be difficult
438 to interpret due to its pleiotropic effects. RecA is the principal recombinase and
439 induces the complex SOS response resulting in the induction of UvrD expression (100,
440 101). Furthermore, UvrD removes RecA from RecA-DNA complexes, thus functioning
441 as an antirecombinase (102–104). Dissecting these functions of UvrD from other
442 effects that a *recA* mutation may have on the cell would be difficult. Applying the
443 perturbations in combination, i.e. double knockdowns or knockdowns plus rifampicin,
444 would likely lead to confusing results since too many deleterious perturbations may be
445 lethal or change normal cell function too radically to be biologically relevant in the
446 intended way.
447 For the suite of mutant strains investigated we found small but significant
448 changes in colocalisation of UvrD with the replication fork, implying that UvrD is
449 recruited to the replication fork by the frequent blocks to replication it encounters. For
450 example, the UvrD-RNAP interaction could localise UvrD to the vicinity of active
451 transcription machinery (50). Since RNA polymerase is the most common replication
452 block, a secondary consequence would be UvrD-fork colocalisation. This is in contrast
453 to the Rep accessory helicase which has a specific interaction partner in the replisome

454 of the replicative helicase DnaB (89). Recent biochemical findings *in vitro* show that
455 blocks to replication occur very frequently (1)(19)(105), potentially accounting for our
456 finding that UvrD colocalises with the fork more frequently than Rep, despite Rep
457 having a specific interaction partner at the fork.

458 We have shown that replication forks stalled at transcriptional blocks can be
459 rescued by addition of UvrD, prior to or post-stalling. If UvrD is to help perform this
460 function then it must be present during the resolution of collision between the
461 replication and transcription machinery, however, our estimate for dwell time at the
462 fork of just a few milliseconds (compared to seconds for DnaQ (79)) suggests a non-
463 negligible dissociation constant; UvrD is not processive *per se* but rather undergoes
464 rapid turnover at the fork such that there is a high likelihood for UvrD being present at
465 any given time, but not necessarily the same set of molecules. Interestingly we
466 observed a similar dwell time for Rep (13), despite it having a clear association partner
467 in DnaB at the fork. However, using a defective restriction enzyme EcoRI E111G block
468 produced a different effect, with late UvrD addition improving block resolution. This
469 restriction enzyme block is artificial and less biologically relevant but may indicate that
470 the known specific UvrD interaction with RNAP is important. Improved replication
471 resolution with late addition of UvrD is intriguing, implying increased affinity for or
472 activity at pre-stalled replication forks compared to UvrD being present as the fork
473 stalls. Complete understanding requires further study of replication block resolution in
474 different conditions.

475 Our results suggest a model where UvrD diffuses and transiently interacts with
476 DNA at random or through specific interactions such as with RNAP or a specific
477 conformation of the blocked replication fork. At the DNA, UvrD is predominantly
478 tetrameric, either pre-assembling in solution or on the DNA itself. The frequent
479 sampling leads to UvrD often being in the vicinity of the replisome, allowing UvrD to
480 resolve the frequent blocks to replication. It is also possible that certain barriers to
481 replication may be harder for Rep to resolve, and such barriers can possibly be more
482 efficiently removed by UvrD, however, it is still likely to be the case that they do not
483 directly challenge the ability of the cell to replicate the genome in light of *uvrD* deletion
484 still resulting in viable cells. Indeed, UvrD shares a high degree of structural similarity
485 with Rep, although the two proteins differ significantly in their amino acid sequences
486 (31, 106). While Rep is recruited to the fork through specific interactions with DnaB,

487 no such interaction could be identified for UvrD. Stochastic impairment of the ability of
488 Rep to interact with DnaB may necessitate block processing at the fork by UvrD. In
489 summary, our results highlight the contribution of UvrD action to facilitating accurate
490 genome duplication at active replisomes.

491 **MATERIALS AND METHODS**

492 **Strain construction**

493 All strains used in this study (listed in full in SI Table S1, with associated plasmids
494 and primers in SI Tables S2 and S3) are derivatives of the laboratory wild type strain
495 TB28. Tagging of *dnaQ-mCherry-<kan>* (C-terminally labelled) is described in (13).
496 *mGFP-uvrD-<kan>* (N-terminally labelled) was amplified from plasmid pAS79 (*uvrD*$^{+}$)
497 with primers oAS145 and oJGB383 having 50 bp homology to either end of the
498 native *uvrD* locus. The resulting PCR product had homology either side such that
499 recombination with the chromosome would result in integration of the PCR product at
500 the native locus under the control of the native promoter. Prior to integration, all PCR
501 products were treated with DpnI, gel purified, and introduced by electroporation into
502 cells expressing the lambda Red genes from the plasmid pKD46 (55). The
503 recombinants were selected for kanamycin resistance and screened for ampicillin
504 sensitivity. The colonies obtained were verified for integration by PCR and
505 sequencing. The *uvrD* recombinants were verified by PCR amplification using
506 primers oPM319 and oPM320, and sequencing using the primers oJGB417,
507 oJGB418, oPM407, oPM409, oPM411, and oMKG71. Where required, the
508 kanamycin resistance gene was removed by expressing Flp recombinase from the
509 plasmid pCP20 (58) to generate kanamycin sensitive strains carrying the fluorescent
510 protein (FP) fusions. Dual labelled strains were created by introducing the kanamycin
511 tagged FP alleles by standard P1 mediated transduction into single labelled strains
512 carrying the required FP allele after removing the linked kanamycin marker.

513 **Determination of cell doubling time**

514 *E. coli* strains were grown overnight in LB medium at 37°C at 200 rpm shaking. The
515 saturated overnight cultures were diluted 100 fold into fresh LB or washed once with
516 1X 56 salts and diluted 100 fold in fresh 1X 56 salts with 0.2% glucose as the carbon
517 source. Aliquots of 100 µl each of the diluted cultures in fresh media were pipetted

518 into individual wells of 96 well clear flat bottom sterile microplates (Corning). The
519 microplates containing the diluted cultures were incubated in a BMG LABTECH
520 SPECTROstar Nano microplate reader at 37°C and the optical density (A_{600}) values
521 were recorded at defined time intervals. The time taken for the optical density values
522 to increase two fold during the exponential growth phase of the culture was taken as
523 the cell doubling time (SI Table S4, Supplementary Figure S1).

524 **Protein Overexpression and Purification**

525 *mGFP-uvrD* was excised from pAS79 using XhoI and SalI and ligated into pET14b
526 cut with XhoI, creating pAS152 encoding N-terminal histidine-tagged mGFP-UvrD.
527 pAS152 was used to overexpress the mGFP-UvrD fusion in Rosetta™
528 2(DE3)/pLysS. The cells were grown in LB medium containing 100 µg/ml ampicillin
529 and 30 µg/ml chloramphenicol at 37ºC and 220 rpm to OD_{600} ~ 0.7. The cultures
530 were then equilibrated to room temperature and overexpression was induced by
531 adding 1 mM IPTG and incubating at 16ºC for 24 hours. Cells from the expressed
532 culture were collected by centrifugation at 4ºC and frozen at -80ºC. The cells were
533 later thawed on ice and resuspended in buffer A (20 mM Tris-Cl pH 8.3, 500 mM
534 NaCl, 5 mM imidazole, 10% glycerol) along with 0.1 mg/ml lysozyme, 1 mM AEBSF,
535 0.7 µg/ml pepstatin, 0.5 µg/ml leupeptin, 2.5 µg/ml DNase I and 20 µg/ml RNase A
536 and incubated on ice for 30 minutes. Brij-58 was then added to a final concentration
537 of 0.1% v/v and incubated on ice for another 20 minutes. The suspension was
538 sonicated and then clarified by centrifugation at 18,000 rpm for 60 minutes at 4ºC in
539 an SS-34 rotor to remove debris. The lysate containing mGFP-UvrD was applied to a
540 5 ml His-trap FF crude column (GE healthcare) and the protein was purified by
541 chromatography on an imidazole gradient in buffer A. Peak fractions were collected
542 and concentrated using a Vivaspin 500 concentrator (30 kDa MWCO) (Sartorius).
543 Samples were then aliquoted and flash frozen in liquid nitrogen before storage at -
544 80ºC. Protein concentration was determined by Bradford's assay.

545 UvrD was purified as previously described (59). Briefly UvrD was overexpressed in
546 BL21-AI from a pETDuet vector, via induction by IPTG and arabinose. UvrD was
547 purified from the soluble cell extract after lysis through the use of affinity (heparin
548 agarose), anion exchange (Q-sepharose), and gel filtration chromatography. Pure
549 UvrD was then stored at -80ºC after dialysis into storage buffer or used immediately

550 in Size Exclusion Chromatography - Multi-Angle Laser Light Scattering (SEC-
551 MALLS) analysis.

552 Biotinylated UvrD and Rep were purified as previously described (60). Briefly, the
553 proteins were overexpressed in a BL21 (DE3) containing pBirAcm, encoding a biotin
554 ligase via induction by IPTG and the addition of biotin to the growth media. The
555 biotinylated proteins were then purified from the soluble cell extracts by ammonium
556 sulphate precipitation, and affinity chromatography (softlink avidin and heparin
557 agarose). Pure proteins were then dialysed into storage buffer overnight and stored
558 at -80°C

559 **Helicase assay**

560 Assays for unwinding of streptavidin-bound forks were performed using a substrate
561 made by annealing oligonucleotides oPM187B20 (5' end labelled with ^{32}P) and
562 oPM188B34. Reactions were performed in 10 µL volumes containing 40 mM HEPES
563 (pH 8); 10 mM DTT; 10 mM magnesium acetate; 2 mM ATP; 0.1 mg ml^{-1} BSA and
564 1 nM forked DNA substrate. Reactions were carried out as described earlier (13, 61).
565 Briefly, the reaction mixture was pre-incubated at 37°C for five minutes with or
566 without 1 µM streptavidin (Sigma-Aldrich), to which helicase (as indicated) and biotin
567 (Sigma-Aldrich) were added to 100 µM (acting as a trap for free streptavidin) and
568 incubated at 37°C for another 10 minutes. Reactions were stopped by addition of 2.5
569 µl of 2.5% SDS, 200 mM EDTA and 10 mg ml^{-1} of proteinase K. Reactions were then
570 analysed by non-denaturing gel electrophoresis on 10% polyacrylamide TBE gels.
571 The quantification of the unwinding and displacement of streptavidin from the fork
572 was carried out as described in (62).

573 **Preparation of cells for microscopy**

574 Cells were grown overnight in LB to saturation. The overnight cultures were
575 inoculated the next day at 1:1000 dilution in 1X 56 salts supplemented with 0.2%
576 glucose as the carbon source. The dilutions were then grown at 30°C to mid-log
577 phase.

578 **Rifampicin treatment**

579 Cells prepared for microscopy were treated with rifampicin at a final concentration of
580 50 µg/mL for 30 minutes at 30°C.

581 **Microscopy and image analysis**

582 Imaging was performed on a bespoke dual-colour single-molecule microscope (13).
583 Excitation from Obis 488 nm and 561 nm wavelength 50mW lasers (run at 20 mW)
584 was reduced to 10 µm at full width half maximum field in the sample plane producing
585 Slimfield illumination (63) producing a mean excitation intensity of ~0.25 mW/µm^2.
586 Lasers were digitally modulated to 5 ms period to produce alternating laser excitation
587 using National Instruments dynamic I/O module NI 9402. Excitation was coupled into
588 a Zeiss microscope body with the sample mounted on a Mad City Labs nanostage.
589 Images were magnified to 80nm/pixel and imaged using an Andor Ixon 128 emCCD
590 camera. Colour channels were split red/green using a bespoke colour splitter
591 consisting of a dual-pass green/red dichroic mirror centred at long-pass wavelength
592 560 nm and emission filters with 25 nm bandwidths centred at 542 nm and 594 nm.

593 Cells were imaged on agarose pads suffused with minimal media as described
594 previously (64). Foci were detected and tracked using previously described bespoke
595 MATLAB software (65). In brief, bright candidate foci were detected in each frame by
596 image transformation and thresholding. A 17x17 pixel region of interest (ROI) is
597 drawn around each candidate and subjected to iterative Gaussian masking (66). Foci
598 were accepted if their signal to noise ratio was above 0.4. Foci in successive frames
599 were linked together into trajectories based on nearest distance, provided it was < 5
600 pixels. Linked foci were accepted as “tracks” nominally if they persist for at least 4
601 consecutive image frames.

602 Characteristic intensity of mGFP or mCherry was determined from the distribution of
603 foci intensity values towards the end of the photobleach confirmed by overtracking
604 foci beyond their bleaching and applying an edge-preserving filter (67, 68) to the raw
605 intensity data to generate individual steps of the characteristic intensity, due to
606 photobleaching (Supplementary Figure S7). This intensity was used to determine the
607 stoichiometry of foci by fitting the first 3 intensity points with a straight line and
608 dividing the intercept by this characteristic intensity. The number of peaks in the
609 Gaussian fits to UvrD was set by running a peak fitting algorithm over the wild type
610 distribution. This number of Gaussians was then used for mutant distributions unless

611 two or more of the Gaussians converged on the same/similar peak value, in which
612 case they were removed. For DnaQ, two peaks were fit as used previously (69).

613 GFP and mCherry images were aligned based on the peak of the 2D cross
614 correlation between their respective brightfield images. Colocalisation between foci
615 and the probability of random colocalisation was determined as described previously
616 (70, 71).

617 The microscopic apparent diffusion coefficients (*D*) were determined by fitting a
618 straight line to the first three mean squared displacements (MSD) values constrained
619 through the equivalent localization precision MSD as determined from the intensity
620 (72, 73). *D* distributions were fit by three Gamma distributions as described
621 previously (74–76). Dwell time was calculated as the number of frames that each
622 trajectory was colocalised with the fork position, as determined by the DnaQ foci
623 detected at time zero.

624 **SEC-MALLS**

625 Size Exclusion Chromatography – Multi-Angle Laser Light Scattering (SEC-MALLS)
626 experiments used Wyatt HELEOS-II multi-angle light scattering and rEX refractive
627 index detectors linked to a Shimadzu HPLC system (SPD-20A UV detector, LC20-
628 AD isocratic pump system, DGU-20A3 degasser and SIL-20A autosampler) with a
629 G.E. Superdex S200 10/300 column at a flow rate of 0.5 mL/min in buffer of 20 mM
630 Tris pH 8.3 (at 4degC) 1 mM EDTA, 1 mm EGTA, 1 mM DTT, 200 mM NaCl, 5%
631 glycerol buffer. Data were analysed using Wyatt Astra 7 software. MWs were
632 estimated using the Zimm fit method with degree 1. A value of 0.182 mL/g was used
633 for protein refractive index increment (dn/dc).

634 **Surface plasmon resonance (SPR)**

635 SPR was performed at 25°C on a BIAcore T200 instrument as in (12). Immobilisation
636 of *E. coli* UvrD and Rep was performed onto streptavidin-coated SA sensor chips
637 whilst the indicated concentrations of Tau and UvrB were passed over in 10 mM
638 HEPES pH 7.4, 3 mM EDTA, 150 mM NaCl, 10 mM $MgCl_2$ and 0.005% Tween 20 at
639 20 µl min^{-1}. This buffer differed from that used in the DNA replication assays to
640 minimise non-specific interactions with the surface-immobilised streptavidin.

641 **Replication assay**

642 Replication assays were carried out using pPM872 as the template for RNAP blocks
643 (1) or pPM594 (12) for EcoRI E111G blocks. Plasmid pPM872 contains $P_{lacUV5\ 52C}$, a
644 strong promoter in which the first 52 nucleotides of the transcript lack cytosine
645 residues and are then followed by four consecutive cytosines. This enables
646 transcription of $P_{lacUV5\ 52C}$ to be stalled by the omission of CTP. Assays were
647 performed in 40 mM HEPES (pH 8); 10 mM DTT; 10 mM magnesium acetate; 2 mM
648 ATP; 0.2 mM GTP, 0.2 mM UTP; 0.04 mM dNTPs; and 0.1 mg/ml BSA. Reactions
649 (15 µl) contained 2 nM plasmid template, 50 nM DNA polymerase III αεθ complex,
650 25 nM τ clamp loader complex, 160 nM DnaB and DnaC monomers, 1 µM SSB, 80
651 nM β clamp, 30 nM HU, 200 nM DnaG, 300 nM DnaA. Helicases were added as
652 indicated. Rep and UvrD used at 200 nM. *E. coli* RNAP holoenzyme from NEB (1
653 U/µl) was used at 1/3 dilution. Dilution was determined empirically to match RNAP
654 replication inhibition levels from (1). EcoRI E111G was purified as in (77) and used
655 at 200 nM. Reactions were assembled on ice and initiated by addition of DnaA and
656 incubation for 4 min at 37°C, followed by addition of 60 units SmaI (Promega) plus
657 0.4 MBq [α^{32}P] dCTP (222 TBq/mmol). Standard reactions with the helicase present
658 in the initial protein mix were carried out at 37°C for 1 minute and then terminated by
659 addition of 1 µl of 0.5 M EDTA. Delayed helicase addition was carried out by adding
660 Rep/UvrD after 1 minute and incubation for a further minute at 37°C before
661 termination with EDTA. Ethanol precipitated replication products were analysed by
662 denaturing agarose gel electrophoresis (0.7% agarose in 2 mM EDTA, 30 mM NaOH
663 for 400 volt hours, standard run was 16 hours at 25 V), phosphorimaging and
664 autoradiography. 5'-labelled HindIII- digested lambda DNA was used as a marker.
665 Gels were quantified using Quantity One® (Bio-Rad) software. Full-length plasmid
666 replication products were quantified as a proportion of summed blocked products
667 and normalised for length (for EcoRI E111G block), or total lane signal (RNAP
668 block).

669

670 **Acknowledgments**

671 We thank Maria Chechik for help with mGFP-UvrD purification. We thank Prof. Nigel
672 Savery (University of Bristol) for the gift of the pETDuet-UvrD overexpression plasmid.

We thank the Molecular Interactions Laboratory in the Bioscience Technology Facility at the University of York for technical assistance and support.

Funding

Supported by BBSRC via grants BB/N006453/1 (M.L., P.M.), BB/R001235/1 (M.L., (M.L.,P.M.,A.S.), BB/N014863/1 (M.H.).

683 **REFERENCES**
684

685 1. M. Hawkins, *et al.*, Direct removal of RNA polymerase barriers to replication by
686 accessory replicative helicases. *Nucleic Acids Res.* **47** (2019).
687 2. R. T. Pomerantz, M. O'Donnell, The replisome uses mRNA as a primer after
688 colliding with RNA polymerase. *Nature* **456**, 762–767 (2008).
689 3. H. Merrikh, C. Machón, W. H. Grainger, A. D. Grossman, P. Soultanas, Co-
690 directional replication-transcription conflicts lead to replication restart. *Nature*
691 **470**, 554–7 (2011).
692 4. A. H. Syeda, J. Atkinson, R. G. Lloyd, P. McGlynn, The balance between
693 recombination enzymes and accessory replicative helicases in facilitating
694 genome duplication. *Genes (Basel).* **7** (2016).
695 5. A. Helmrich, M. Ballarino, L. Tora, Collisions between replication and
696 transcription complexes cause common fragile site instability at the longest
697 human genes. *Mol. Cell* **44**, 966–977 (2011).
698 6. Y. Takeuchi, T. Horiuchi, T. Kobayashi, Transcription-dependent
699 recombination and the role of fork collision in yeast rDNA. *Genes Dev.* **17**,
700 1497–1506 (2003).
701 7. A. L. de Septenville, S. Duigou, H. Boubakri, B. Michel, Replication fork
702 reversal after replication-transcription collision. *PLoS Genet.* **8** (2012).
703 8. C. J. Rudolph, A. L. Upton, A. Stockum, C. A. Nieduszynski, R. G. Lloyd,
704 Avoiding chromosome pathology when replication forks collide. *Nature* **500**,
705 608–611 (2013).
706 9. B. Michel, G. Grompone, M. J. Florès, V. Bidnenko, Multiple pathways process
707 stalled replication forks. *Proc. Natl. Acad. Sci. U. S. A.* **101**, 12783–12788
708 (2004).
709 10. E. V. Mirkin, S. M. Mirkin, Mechanisms of transcription-replication collisions in
710 bacteria. *Mol. Cell. Biol.* **25**, 888–895 (2005).
711 11. P. McGlynn, N. J. Savery, M. S. Dillingham, The conflict between DNA
712 replication and transcription. *Mol. Microbiol.* **85**, 12–20 (2012).
713 12. C. P. Guy, *et al.*, Rep provides a second motor at the replisome to promote
714 duplication of protein-bound DNA. *Mol. Cell* **36**, 654–666 (2009).
715 13. A. H. Syeda, *et al.*, Single-molecule live cell imaging of Rep reveals the
716 dynamic interplay between an accessory replicative helicase and the
717 replisome. *Nucleic Acids Res.* **47**, 6287–6298 (2019).
718 14. P. McGlynn, Linking transcription with DNA repair, damage tolerance, and
719 genome duplication. *Proc. Natl. Acad. Sci. U. S. A.* **107**, 15314–15315 (2010).
720 15. D. Dutta, K. Shatalin, V. Epshtein, M. E. Gottesman, E. Nudler, Linking RNA
721 polymerase backtracking to genome instability in E. coli. *Cell* **146**, 533–543
722 (2011).
723 16. D. Duchi, *et al.*, RNA Polymerase Pausing during Initial Transcription. *Mol. Cell*
724 **63**, 939–950 (2016).
725 17. G. Ghosal, J. Chen, DNA damage tolerance: a double-edged sword guarding
726 the genome. *Transl. Cancer Res.* **2**, 107–129 (2013).
727 18. S. Hamperl, M. J. Bocek, J. C. Saldivar, T. Swigut, K. A. Cimprich,
728 Transcription-Replication Conflict Orientation Modulates R-Loop Levels and
729 Activates Distinct DNA Damage Responses. *Cell* **170**, 774-786.e19 (2017).
730 19. K. Hizume, H. Araki, Replication fork pausing at protein barriers on
731 chromosomes. *FEBS Lett.* **593**, 1449–1458 (2019).
732 20. K. K. Myka, M. E. Gottesman, DksA and DNA double-strand break repair.

733 *Curr. Genet.* **65**, 1297–1300 (2019).
734 21. K. K. Myka, *et al.*, Inhibiting translation elongation can aid genome duplication
735 in Escherichia coli. *Nucleic Acids Res.* **45**, 2571–2584 (2017).
736 22. S. M. Mangiameli, C. N. Merrikh, P. A. Wiggins, H. Merrikh, Transcription leads
737 to pervasive replisome instability in bacteria. *Elife* **6** (2017).
738 23. V. Kamarthapu, *et al.*, ppGpp couples transcription to DNA repair in E. coli.
739 *Science* **352**, 993–996 (2016).
740 24. B. J. Brewer, When polymerases collide: replication and the transcriptional
741 organization of the E. coli chromosome. *Cell* **53**, 679–686 (1988).
742 25. A. Srivatsan, A. Tehranchi, D. M. MacAlpine, J. D. Wang, Co-orientation of
743 replication and transcription preserves genome integrity. *PLoS Genet.* **6**
744 (2010).
745 26. B. Liu, B. M. Alberts, Head-on collision between a DNA replication apparatus
746 and RNA polymerase transcription complex. *Science* **267**, 1131–1137 (1995).
747 27. J. D. Wang, M. B. Berkmen, A. D. Grossman, Genome-wide coorientation of
748 replication and transcription reduces adverse effects on replication in Bacillus
749 subtilis. *Proc. Natl. Acad. Sci. U. S. A.* **104**, 5608–5613 (2007).
750 28. T. S. Sankar, B. D. Wastuwidyaningtyas, Y. Dong, S. A. Lewis, J. D. Wang,
751 The nature of mutations induced by replication–transcription collisions. *Nature*
752 **535**, 178–181 (2016).
753 29. D. Ivanova, *et al.*, Shaping the landscape of the Escherichia coli chromosome:
754 replication-transcription encounters in cells with an ectopic replication origin.
755 *Nucleic Acids Res.* **43**, 7865–7877 (2015).
756 30. A. Helmrich, M. Ballarino, E. Nudler, L. Tora, Transcription-replication
757 encounters, consequences and genomic instability. *Nat. Struct. Mol. Biol.* **20**,
758 412–418 (2013).
759 31. J. G. Brüning, J. L. Howard, P. McGlynn, Accessory replicative helicases and
760 the replication of protein-bound DNA. *J. Mol. Biol.* **426**, 3917–3928 (2014).
761 32. K. R. McDonald, *et al.*, Pfh1 Is an Accessory Replicative Helicase that
762 Interacts with the Replisome to Facilitate Fork Progression and Preserve
763 Genome Integrity. *PLoS Genet.* **12** (2016).
764 33. J. E. Sokoloski, A. G. Kozlov, R. Galletto, T. M. Lohman, Chemo-mechanical
765 pushing of proteins along single-stranded DNA. *Proc. Natl. Acad. Sci. U. S. A.*
766 **113**, 6194–6199 (2016).
767 34. G. D. Schauer, *et al.*, Replisome bypass of a protein-based R-loop block by
768 Pif1. *Proc. Natl. Acad. Sci. U. S. A.* **117**, 30354–30361 (2020).
769 35. M. K. Gupta, *et al.*, Protein-DNA complexes are the primary sources of
770 replication fork pausing in Escherichia coli. *Proc. Natl. Acad. Sci. U. S. A.* **110**,
771 7252–7257 (2013).
772 36. H. Boubakri, A. L. De Septenville, E. Viguera, B. Michel, The helicases DinG,
773 Rep and UvrD cooperate to promote replication across transcription units in
774 vivo. *EMBO J.* **29**, 145–157 (2010).
775 37. X. Liu, J. X. Seet, Y. Shi, P. R. Bianco, Rep and UvrD Antagonize One Another
776 at Stalled Replication Forks and This Is Exacerbated by SSB. *ACS Omega* **4**,
777 5180–5196 (2019).
778 38. O. Adebali, Y. Y. Chiou, J. Hu, A. Sancar, C. P. Selby, Genome-wide
779 transcription-coupled repair in Escherichia coli is mediated by the Mfd
780 translocase. *Proc. Natl. Acad. Sci. U. S. A.* **114**, E2116–E2125 (2017).
781 39. N. Kang, E. Choi, S. G. Kim, J. Hwang, Inhibitory effect of UvrD and DinG on
782 the replication of ColE1-derived plasmids in Escherichia coli. *Plasmid* **81**, 32–

783 41 (2015).
784 40. V. Epshtein, UvrD helicase: an old dog with a new trick: how one step
785 backward leads to many steps forward. *Bioessays* **37**, 12–19 (2015).
786 41. P. R. Caron, S. R. Kushner, L. Grossman, Involvement of helicase II (uvrD
787 gene product) and DNA polymerase I in excision mediated by the uvrABC
788 protein complex. *Proc. Natl. Acad. Sci. U. S. A.* **82**, 4925–4929 (1985).
789 42. B. Van Houten. Nucleotide excision repair in Escherichia coli. *Microbiol. Rev.*
790 **54**, 18–51 (1990).
791 43. A. L. Lu, S. Clark, P. Modrich, Methyl-directed repair of DNA base-pair
792 mismatches in vitro. *Proc. Natl. Acad. Sci. U. S. A.* **80**, 4639–4643 (1983).
793 44. S. W. Matson, A. B. Robertson, The UvrD helicase and its modulation by the
794 mismatch repair protein MutL. *Nucleic Acids Res.* **34**, 4089–4097 (2006).
795 45. L. Manelyte, *et al.*, The unstructured C-terminal extension of UvrD interacts
796 with UvrB, but is dispensable for nucleotide excision repair. *DNA Repair*
797 *(Amst).* **8**, 1300–1310 (2009).
798 46. A. B. Robertson, S. R. Pattishall, E. A. Gibbons, S. W. Matson, MutL-catalyzed
799 ATP hydrolysis is required at a post-UvrD loading step in methyl-directed
800 mismatch repair. *J. Biol. Chem.* **281**, 19949–19959 (2006).
801 47. E. J. Gwynn, *et al.*, The conserved C-terminus of the PcrA/UvrD helicase
802 interacts directly with RNA polymerase. *PLoS One* **8** (2013).
803 48. K. Sanders, *et al.*, The structure and function of an RNA polymerase
804 interaction domain in the PcrA/UvrD helicase. *Nucleic Acids Res.* **45**, 3875–
805 3887 (2017).
806 49. V. Epshtein, *et al.*, UvrD facilitates DNA repair by pulling RNA polymerase
807 backwards. *Nature* **505**, 372–377 (2014).
808 50. B. K. Bharati, *et al.*, Crucial role and mechanism of transcription-coupled DNA
809 repair in bacteria. *Nature* **604**, 152–159 (2022).
810 51. B. Martinez, B. K. Bharati, V. Epshtein, E. Nudler, Pervasive Transcription-
811 coupled DNA repair in E. coli. *Nat. Commun.* **13** (2022).
812 52. N. M. Haines, Y. I. T. Kim, A. J. Smith, N. J. Savery, Stalled transcription
813 complexes promote DNA repair at a distance. *Proc. Natl. Acad. Sci. U. S. A.*
814 **111**, 4037–4042 (2014).
815 53. A. J. Smith, N. J. Savery, Effects of the bacterial transcription-repair coupling
816 factor during transcription of DNA containing non-bulky lesions. *DNA Repair*
817 *(Amst).* **7**, 1670–1679 (2008).
818 54. A. J. Smith, N. J. Savery, RNA polymerase mutants defective in the initiation of
819 transcription-coupled DNA repair. *Nucleic Acids Res.* **33**, 755–764 (2005).
820 55. J. Atkinson, *et al.*, Stimulation of UvrD helicase by UvrAB. *J. Biol. Chem.* **284**,
821 9612–9623 (2009).
822 56. R. P. Wong, N. García-Rodríguez, N. Zilio, M. Hanulová, H. D. Ulrich,
823 Processing of DNA Polymerase-Blocking Lesions during Genome Replication
824 Is Spatially and Temporally Segregated from Replication Forks. *Mol. Cell* **77**,
825 3-16.e4 (2020).
826 57. N. K. Maluf, T. M. Lohman, Self-association equilibria of Escherichia coli UvrD
827 helicase studied by analytical ultracentrifugation. *J. Mol. Biol.* **325**, 889–912
828 (2003).
829 58. K. A. Datsenko, B. L. Wanner, One-step inactivation of chromosomal genes in
830 Escherichia coli K-12 using PCR products. *Proc. Natl. Acad. Sci. U. S. A.* **97**,
831 6640–6645 (2000).
832 59. J. Atkinson, *et al.*, Stimulation of UvrD helicase by UvrAB. *J. Biol. Chem.* **284**,

833 9612–9623 (2009).
834 60. C. P. Guy, *et al.*, Rep provides a second motor at the replisome to promote
835 duplication of protein-bound DNA. *Mol. Cell* **36**, 654–666 (2009).
836 61. J. G. Brüning, J. A. L. Howard, K. K. Myka, M. S. Dillingham, P. McGlynn, The
837 2B subdomain of Rep helicase links translocation along DNA with protein
838 displacement. *Nucleic Acids Res.* **46**, 8917–8925 (2018).
839 62. J. G. Brüning, J. A. L. Howard, P. McGlynn, Use of streptavidin bound to
840 biotinylated DNA structures as model substrates for analysis of nucleoprotein
841 complex disruption by helicases. *Methods* **108**, 48–55 (2016).
842 63. M. Plank, G. H. Wadhams, M. C. Leake, Millisecond timescale slimfield
843 imaging and automated quantification of single fluorescent protein molecules
844 for use in probing complex biological processes. *Integr. Biol.* **1**, 602–612
845 (2009).
846 64. A. J. M. Wollman, A. H. Syeda, P. McGlynn, M. C. Leake, Single-Molecule
847 Observation of DNA Replication Repair Pathways in E. coli. *Adv. Exp. Med.*
848 *Biol.* **915**, 5–16 (2016).
849 65. H. Miller, *et al.*, Superresolution imaging of single DNA molecules using
850 stochastic photoblinking of minor groove and intercalating dyes. *Methods* **88**,
851 81–8 (2015).
852 66. M. C. Leake, *et al.*, Stoichiometry and turnover in single, functioning
853 membrane protein complexes. *Nature* **443**, 355–358 (2006).
854 67. M. C. Leake, D. Wilson, B. Bullard, R. M. Simmons, The elasticity of single
855 kettin molecules using a two-bead laser-tweezers assay. *FEBS Lett.* **535**, 55–
856 60 (2003).
857 68. M. C. Leake, D. Wilson, M. Gautel, R. M. Simmons, The elasticity of single titin
858 molecules using a two-bead optical tweezers assay. *Biophys. J.* **87**, 1112–35
859 (2004).
860 69. R. Reyes-Lamothe, D. J. Sherratt, M. C. Leake, Stoichiometry and architecture
861 of active DNA replication machinery in Escherichia coli. *Science* **328**, 498–501
862 (2010).
863 70. I. Llorente-Garcia, *et al.*, Single-molecule in vivo imaging of bacterial
864 respiratory complexes indicates delocalized oxidative phosphorylation.
865 *Biochim. Biophys. Acta* **1837**, 811–24 (2014).
866 71. A. J. M. Wollman, *et al.*, Critical roles for EGFR and EGFR-HER2 clusters in
867 EGF binding of SW620 human carcinoma cells. *J. R. Soc. Interface* **19** (2022).
868 72. A. J. M. Wollman, M. C. Leake, Millisecond single-molecule localization
869 microscopy combined with convolution analysis and automated image
870 segmentation to determine protein concentrations in complexly structured,
871 functional cells, one cell at a time. *Faraday Discuss.* **184**, 401–24 (2015).
872 73. M. C. Leake, *et al.*, Variable stoichiometry of the TatA component of the twin-
873 arginine protein transport system observed by in vivo single-molecule imaging.
874 *Proc. Natl. Acad. Sci. U. S. A.* **105**, 15376–81 (2008).
875 74. H. Miller, *et al.*, High-Speed Single-Molecule Tracking of CXCL13 in the B-
876 Follicle. *Front. Immunol.* **9**, 1073 (2018).
877 75. J. Cosgrove, *et al.*, B cell zone reticular cell microenvironments shape CXCL13
878 gradient formation. *Nat. Commun.* **11** (2020).
879 76. X. Jin, *et al.*, Membraneless organelles formed by liquid-liquid phase
880 separation increase bacterial fitness. *Sci. Adv.* **7** (2021).
881 77. S.-C. Chengs, R. Kim, K. Kings, S.-H. Kim, P. Modrich, Isolation of Gram
882 Quantities of EcoRI Restriction and Modification Enzymes from an

883 Overproducing Strain. *J. Biol. Chem.* **259**, 11571–11575 (1984).
884 78. A. Badrinarayanan, R. Reyes-Lamothe, S. Uphoff, M. C. Leake, D. J. Sherratt,
885 In vivo architecture and action of bacterial structural maintenance of
886 chromosome proteins. *Science* **338**, 528–31 (2012).
887 79. T. R. Beattie, *et al.*, Frequent exchange of the DNA polymerase during
888 bacterial chromosome replication. *Elife* **6**, e21763 (2017).
889 80. R. Reyes-Lamothe, C. Possoz, O. Danilova, D. J. Sherratt, Independent
890 positioning and action of Escherichia coli replisomes in live cells. *Cell* **133**, 90–
891 102 (2008).
892 81. A. L. Payne-Dwyer, A. H. Syeda, J. W. Shepherd, L. Frame, M. C. Leake,
893 RecA and RecB: probing complexes of DNA repair proteins with mitomycin C
894 in live Escherichia coli with single-molecule sensitivity. *bioRxiv*,
895 2021.10.04.463068 (2021).
896 82. D. A. Zacharias, J. D. Violin, A. C. Newton, R. Y. Tsien, Partitioning of lipid-
897 modified monomeric GFPs into membrane microdomains of live cells. *Science*
898 **296**, 913–916 (2002).
899 83. N. K. Maluf, C. J. Fischer, T. M. Lohman, A Dimer of Escherichia coli UvrD is
900 the active form of the helicase in vitro. *J. Mol. Biol.* **325**, 913–935 (2003).
901 84. H. Yokota, Y. A. Chujo, Y. Harada, Single-molecule imaging of the oligomer
902 formation of the nonhexameric Escherichia coli UvrD helicase. *Biophys. J.* **104**,
903 924–933 (2013).
904 85. H. Yokota, Quantitative and kinetic single-molecule analysis of DNA unwinding
905 by Escherichia coli UvrD helicase. *Biophys. physicobiology* **19**, n/a (2022).
906 86. H. M. Arthur, P. B. Eastlake, Transcriptional control of the uvrD gene of
907 Escherichia coli. *Gene* **25**, 309–316 (1983).
908 87. Y. Taniguchi, *et al.*, Quantifying E. coli proteome and transcriptome with
909 single-molecule sensitivity in single cells. *Science* **329**, 533–8 (2010).
910 88. G. W. Li, D. Burkhardt, C. Gross, J. S. Weissman, Quantifying absolute protein
911 synthesis rates reveals principles underlying allocation of cellular resources.
912 *Cell* **157**, 624–635 (2014).
913 89. J. Atkinson, M. K. Gupta, P. McGlynn, Interaction of Rep and DnaB on DNA.
914 *Nucleic Acids Res.* **39**, 1351–1359 (2011).
915 90. S. V. Rajagopala, *et al.*, The binary protein-protein interaction landscape of
916 Escherichia coli. *Nat. Biotechnol. 2014 323* **32**, 285–290 (2014).
917 91. D. K. Orrens, C. P. Selbys, J. E. Hearst, A. Sancars, Post-incision Steps of
918 Nucleotide Excision Repair in Escherichia coli DISASSEMBLY OF THE
919 UvrBC-DNA COMPLEX BY HELICASE I1 AND DNA POLYMERASE I*. *J.
920 Biol. Chem.* **267**, 780–788 (1992).
921 92. P. McGlynn, R. G. Lloyd, Modulation of RNA polymerase by (p)ppGpp reveals
922 a RecG-dependent mechanism for replication fork progression. *Cell* **101**, 35–
923 45 (2000).
924 93. Y. N. Zhou, D. J. Jin, The rpoB mutants destabilizing initiation complexes at
925 stringently controlled promoters behave like “stringent” RNA polymerases in
926 Escherichia coli. *Proc. Natl. Acad. Sci. U. S. A.* **95**, 2908–2913 (1998).
927 94. E. A. Campbell, *et al.*, Structural mechanism for rifampicin inhibition of
928 bacterial rna polymerase. *Cell* **104**, 901–912 (2001).
929 95. M. Stracy, *et al.*, Live-cell superresolution microscopy reveals the organization
930 of RNA polymerase in the bacterial nucleoid. *Proc. Natl. Acad. Sci. U. S. A.*
931 **112**, E4390-9 (2015).
932 96. K. King, S. J. Benkovics, P. Modrich, Glu-11 1 Is Required for Activation of the

933 DNA Cleavage Center of EcoRI Endonuclease*. *J. Biol. Chem.* **264**, 11807–
934 11815 (1989).
935 97. B. Nguyen, Y. Ordabayev, J. E. Sokoloski, E. Weiland, T. M. Lohman, Large
936 domain movements upon UvrD dimerization and helicase activation. *Proc.*
937 *Natl. Acad. Sci.* **114**, 12178–12183 (2017).
938 98. A. Wagner, Robustness against mutations in genetic networks of yeast. *Nat.*
939 *Genet. 2000 244* **24**, 355–361 (2000).
940 99. J. Atkinson, *et al.*, Localization of an accessory helicase at the replisome is
941 critical in sustaining efficient genome duplication. *Nucleic Acids Res.* **39**, 949–
942 957 (2011).
943 100. S. C. Massoni, S. J. Sandler, Specificity in suppression of SOS expression by
944 recA4162 and uvrD303. *DNA Repair (Amst).* **12**, 1072–1080 (2013).
945 101. K. H. Maslowska, K. Makiela-Dzbenska, I. J. Fijalkowska, The SOS system: A
946 complex and tightly regulated response to DNA damage. *Environ. Mol.*
947 *Mutagen.* **60**, 368–384 (2019).
948 102. R. C. Centore, S. J. Sandler, UvrD limits the number and intensities of RecA-
949 green fluorescent protein structures in Escherichia coli K-12. *J. Bacteriol.* **189**,
950 2915–2920 (2007).
951 103. V. Petrova, *et al.*, Active displacement of RecA filaments by UvrD translocase
952 activity. *Nucleic Acids Res.* **43**, 4133–4149 (2015).
953 104. M. M. Cox, Regulation of bacterial RecA protein function. *Crit. Rev. Biochem.*
954 *Mol. Biol.* **42**, 41–63 (2007).
955 105. N. Raghunathan, S. Goswami, J. K. Leela, A. Pandiyan, J. Gowrishankar, A
956 new role for Escherichia coli Dam DNA methylase in prevention of aberrant
957 chromosomal replication. *Nucleic Acids Res.* **47**, 5698–5711 (2019).
958 106. H. Yokota, Roles of the C-Terminal Amino Acids of Non-Hexameric Helicases:
959 Insights from Escherichia coli UvrD. *Int. J. Mol. Sci.* **22**, 1–19 (2021).
960
961
962

963 # Supplementary Information

964 ## Tetrameric UvrD helicase is located at the *E. coli* replisome due to
965 ## frequent replication blocks

966 Adam J. M Wollman[1,2,3,], Aisha H. Syeda[1,2], Jamieson A. L. Howard[1,2], Alex Payne-Dwyer[1,2], Andrew
967 Leech[4] , Colin Guy[5, 6], Peter McGlynn[2,6], Michelle Hawkins[2] and Mark C. Leake[1,2]
968 The authors wish it to be known that, in their opinion, the first two authors should be regarded as joint
969 First Authors
970 [1] School of Physics, Engineering and Technology, University of York, York YO10 5DD, United
971 Kingdom.
972 [2] Department of Biology, University of York, York YO10 5DD, United Kingdom.
973 [3] Current address: Biosciences Institute, Newcastle University, NE1 7RU, United Kingdom.
974 [4] Bioscience Technology Facility, Department of Biology, University of York, York YO10 5DD, United
975 Kingdom
976 [5] Current address: Covance Laboratories Ltd., Otley Road, Harrogate, HG3 1PY, United Kingdom
977 [6] Previous address: School of Medical Sciences, Institute of Medical Sciences, University of
978 Aberdeen, Foresterhill, Aberdeen AB25 2ZD, United Kingdom
979

980 * To whom correspondence should be addressed. To whom correspondence should be addressed.
981 Tel: +44 (0)1904322697. Email: mark.leake@york.ac.uk

982 Present Address: School of Physics, Engineering and Technology, and Department of Biology,
983 University of York, York YO10 5DD, United Kingdom
984
985
986

987 **Supplementary Tables**

988 **Table S1 Strains used in this study**

Strain	Relevant genotype	Source or derivation
BW25113 derivatives:		
BW25113	*rrnB ΔlacZ4787 hsdR514 Δ(araBAD)567 Δ(rhaBAD)568 rph-1*	(1)
JW2703	*ΔmutS::<kan>*	(1)
JW3786	*ΔuvrD::<kan>*	(1)
JW4019	*ΔuvrA::<kan>*	(1)
MG1655 derivatives:		
TB12	*ΔlacIZYA::<kan>*	
TB28	*ΔlacIZYA*	(2, 3)
TB28 derivatives		
N6577	*ΔlacIZYA Δrep::cat*	(4)
N6661	*ΔlacIZYA::<> Δrep::dhfr* / pAM407 (*uvrD*$^+$ *lacZ*$^+$, a pRC7 derivative)	(4)
N6661	*ΔlacIZYA::<> Δrep::dhfr* / pAM407 (*uvrD*$^+$ *lacZ*$^+$, a pRC7 derivative)	(4)
N6644	*ΔlacIZYA::<> uvrD::dhfr Δrep::cat* / pAM407 (*uvrD*$^+$ *lacZ*$^+$, a pRC7 derivative)	(4)
JGB166	*ΔuvrD* / pKD46	JW3786 transformed with pKD46
AS97	TB28/pKD46	(5)
AS446	*dnaQ-mCherry-<kan>*	
AS448	*dnaQ-mCherry-<>*	(5)
AS512	*mGFP-uvrD-<kan>*	*mGFP-uvrD-<kan>* recombineered into JGB166
AS517	*ΔlacIZYA::<> Δrep::cat mGFP-uvrD-<kan>* / pAM407 (*uvrD*$^+$ *lacZ*$^+$, a pRC7 derivative)	N6661 X P1(AS512)
AS564	*dnaQ-mCherry-<kan> rpoB*35*	PM486 X P1(AS446)
AS571	*dnaQ-mCherry-<> rpoB*35*	AS564 to km^S with pCP20
AS580	*dnaQ-mCherry-<> mGFP-uvrD-<kan>*	AS448 X P1(AS512)
AS582	*dnaQ-mCherry-<> mGFP-uvrD-<kan> rpoB*35*	AS571 X P1(AS512)
AS590	*dnaQ-mCherry-<> mGFP-uvrD-<kan> Δrep::cat*	AS580 X P1(N6577)
AS650	*dnaQ-mCherry-<> mGFP-uvrD-<>*	AS580 to km^S with pCP20
AS656	*dnaQ-mCherry-<> mGFP-uvrD-<> ΔuvrA::<kan>*	AS650 X P1(JW4019)
AS658	*dnaQ-mCherry-<> mGFP-uvrD-<> ΔmutS::<kan>*	AS650 X P1(JW2703)

989

990

991 **Table S2 Plasmids used in this study**

Plasmid	Description	Antibiotic	Reference
pCP20	Yeast Flp recominase expression plasmid	Amp	(6)
pKD46	λ Red recombinase expression plasmid	Amp	(6)
pAS79	pUC18 *mGFP-uvrD-<kan>*	Amp, kan	This study
pAS152	pET14b-mGFP uvrD	Amp	This study

992
993

994 **Table S3 Oligonucleotides used in this study**

Primer	Sequence (5' - 3')
oJGB383	TGAATGATTTTTTAGGCCAAATAAGGTGCGCAGCACCGCATCCGGCAACGCATATGAATATCCTCCTTAG
oJGB417	TACAAGACACGTGCTGAAGTC
oJGB418	TGCTAGTTGAACGCTTCCATC
oMKG71	CGGTGCCCTGAATGAACTGC
oPM319	CTTGTTGGATCAGACCGGAAAATG
oPM320	TGGCAACGCTATCCTTTTGTCA
oPM407	GCGGCAGGCAATGTGGTA
oPM409	CCTTTGAGCGTGTGGTGA
oPM411	CAGCGGCTACAAGCTCGG
oPM187B20	GTCGGATCCTCTAGACAGC(BiodT)CCATGATCACTGGCACTGGTAGAATTCGGC
oPM188B34	AACGTCATAGACGATTACATTGCTACATGGAGC(BiodT)GTCTAGAGGATCCGAC
oAS84	CCCGTCTCGATCTGGTGCAG
oAS85	TTGCTGCAAAAATCGCCCAAG
oAS132	CCCGTCTCGATCTGGTGCAGAAGAAAGGCGGAAGTTGCCTCTGGCGAGCAGGCTGGCTCCGCTGCTGG
oAS133	TTGCTGCAAAAATCGCCCAAGTCGCTATTTTTAGCGCCTTTCACAGGTATCATATGAATATCCTCCTTAG
oAS145	AGGGCGTTGCGCTTCTCCGCCCAACCTATTTTTACGCGGCGGTGCCAATGAGTAAAGGAGAAGAACTT

995

996

997 **Table S4 Cell doubling times of labelled strains.** Values expressed are the means of three
998 independent replicates, with standard deviation and standard errors indicated.

Strain (Relevant genotype)	**LB medium**			**Minimal medium**		
	Mean doubling time (min)	**SD (min)**	**SEM (min)**	**Mean doubling time (min)**	**SD (min)**	**SEM (min)**
WT	23.72	1.11	0.64	62.80	17.06	9.85
dnaQ-mCherry	26.85	0.91	0.52	62.22	18.63	10.76
mGFP-uvrD	24.79	0.37	0.22	59.45	1.80	1.04
dnaQ-mCherry mGFP-uvrD	25.27	1.51	0.87	71.03	7.59	4.38
ΔmutS	24.59	0.55	0.32	107.91	13.96	8.06
ΔuvrA	27.99	0.23	0.13	92.25	5.86	3.38
*ΔrpoB*35*	33.98	0.17	0.10	83.11	30.83	17.80
Δrep	24.30	2.03	1.17	62.74	1.20	0.70
dnaQ-mCherry mGFP-uvrD ΔmutS	26.85	0.68	0.39	110.84	34.91	20.16
dnaQ-mCherry mGFP-uvrD ΔuvrA	24.13	0.56	0.33	91.80	5.18	2.99
*dnaQ-mCherry mGFP-uvrD ΔrpoB*35*	32.81	0.70	0.40	99.11	78.68	45.42
dnaQ-mCherry mGFP-uvrD Δrep	26.54	1.90	1.10	62.17	2.98	1.72

999
1000
1001
1002
1003

1004

1005 **Supplementary figures**

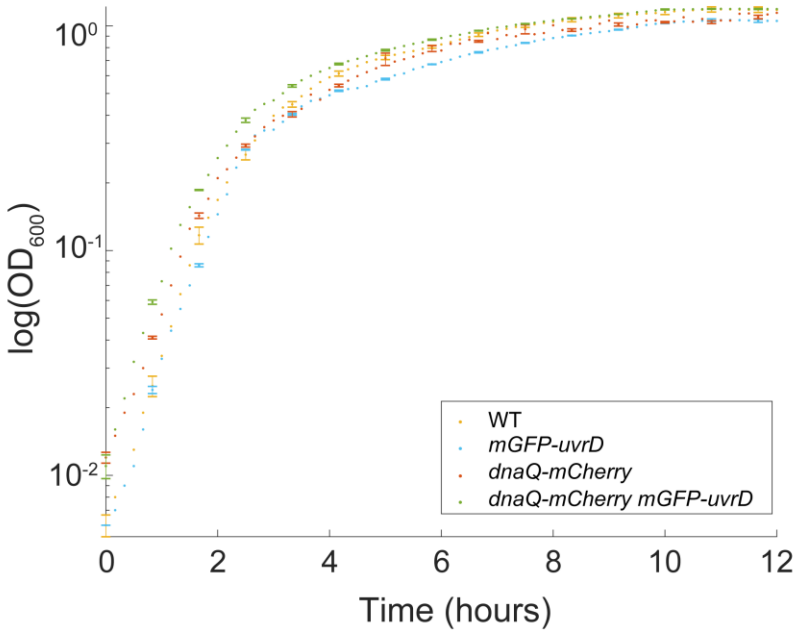

1006

1007

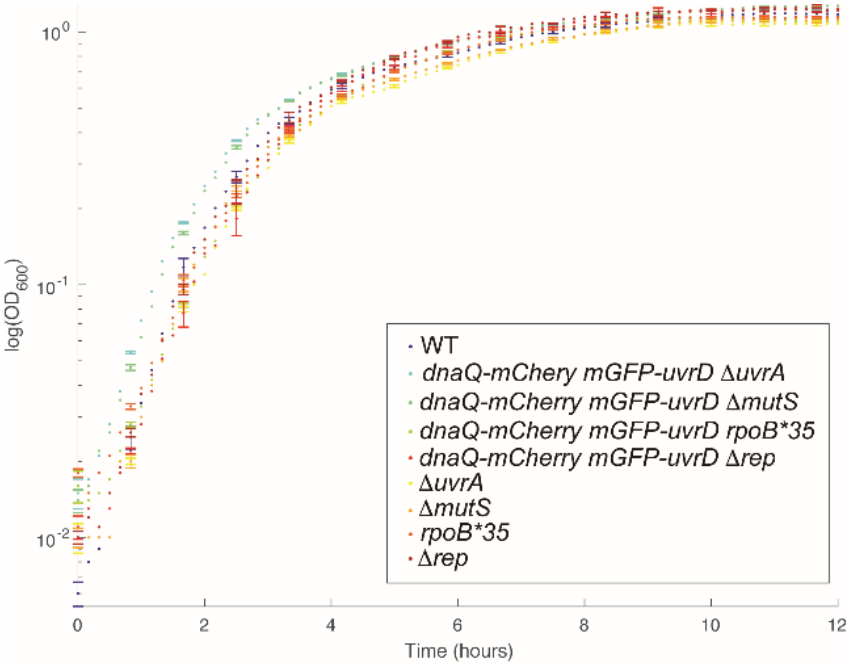

1008

1009 **Supplementary Figure S1. Growth curves in LB medium.** Cultures were grown in LB as
1010 described in the text. The OD_{600} values are plotted on a log scale on the vertical axis with a
1011 linear scale of time in hours on the horizontal axis. The genotypes of the strains are indicated
1012 in boxes within the figures. SD error bars (shown just on every 5th consecutive point for clarity
1013 here), taken from N=3 replicate cultures. Plots in panel A are growth curves of single and dual
1014 labelled wild-type strains, while those in panel B are dual labelled and unlabelled mutant
1015 strains. The unlabelled wild-type strain is included in all panels as a reference.

1016

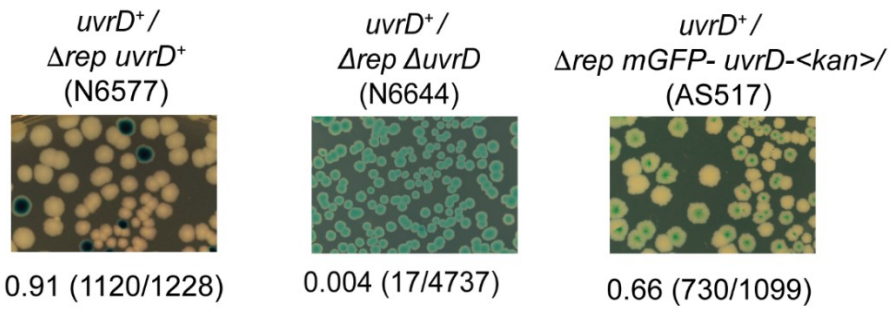

1017

1018 **Supplementary Figure S2: Testing of mGFP-UvrD fusions for retention of function.** We
1019 transformed the strain carrying a chromosomal *mGFP-uvrD* allele with a derivative of pRC7
1020 carrying a wild-type *uvrD* allele (pPM407), which is an unstable low copy plasmid that also
1021 carries the *lacZYA* genes (3). Presence of this plasmid confers blue colour to the colonies on
1022 plates containing Xgal when strains are chromosomally deleted for the *lac* operon. In rapidly
1023 growing cells, cells require either *rep* or *uvrD* for viability, and the loss of both is lethal (4, 7).
1024 Thus, *Δrep* cells with a functional *uvrD* allele are viable and can lose pRC7*uvrD*, evidenced
1025 by appearance of white colonies on LB Xgal IPTG plates, but cells lacking *uvrD* function
1026 cannot survive upon loss of the plasmid resulting in recovery of only blue colonies. The *Δrep*
1027 *mGFP-uvrD* cells produced white colonies on Xgal media, indicating that the *mGFP-uvrD*
1028 fusion is functional.

1029

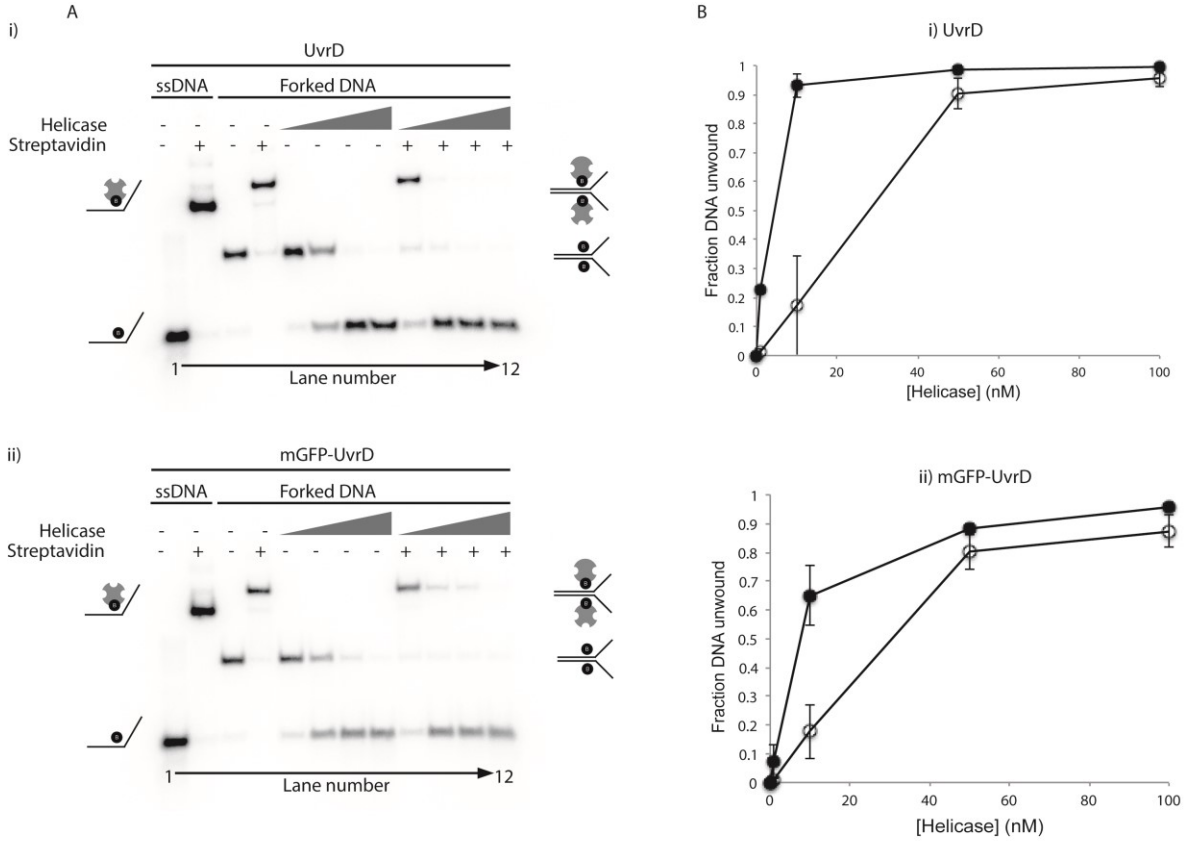

Supplementary Figure S3: mGFP-UvrD fusion is functional *in vitro*. (A) Representative native polyacrylamide TBE gels showing (i) UvrD and (ii) mGFP-UvrD unwinding of forked DNA containing biotin on both strands within the duplex region (8, 9). Lanes 1-4 contain markers indicating the position of single stranded or forked DNA +/- streptavidin as indicated. Lanes 5-12 contain the products of unwinding the forked DNA +/- streptavidin by the indicated helicase at 1, 10, 50 and 100 nM. (B) Quantification of the unwinding of the forked substrate in the absence of (open circles) and presence of (closed circles) streptavidin by the indicated helicases. Data points shown are averages of band intensities (taken from two gels in UvrD and four gels in mGFP-UvrD) with standard errors indicated by bars on the points.

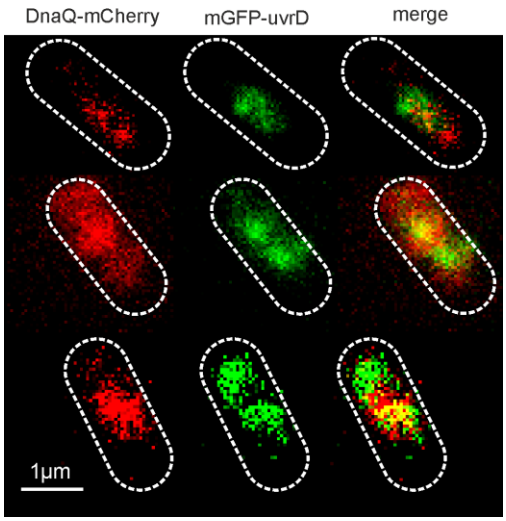

Supplementary Figure S4: Dual colour Slimfield images of mGFP-UvrD:DnaQ-mCherry, scale bar 1 micron. Segmented outlines of cell bodies indicated (white dash).

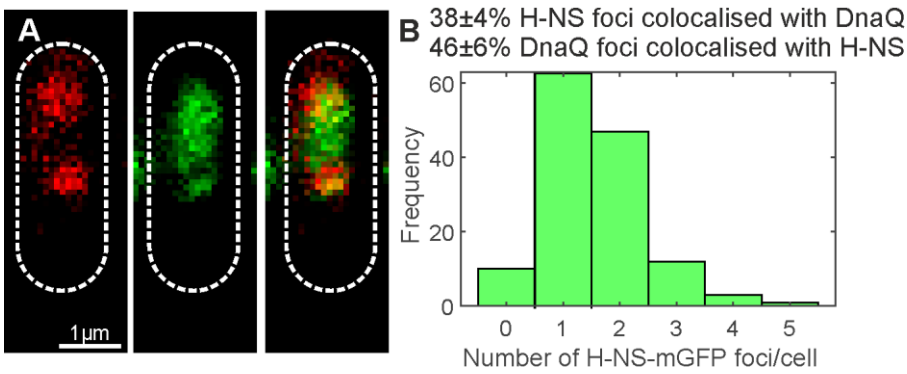

Supplementary Figure S5: (A) Dual colour Slimfield images of H-NS-mGFP-:DnaQ-mCherry, scale bar 1 micron. Segmented outlines of cell bodies indicated (white dash). (B) Histogram showing the number of H-NS foci detected per cell, SD errors.

1049

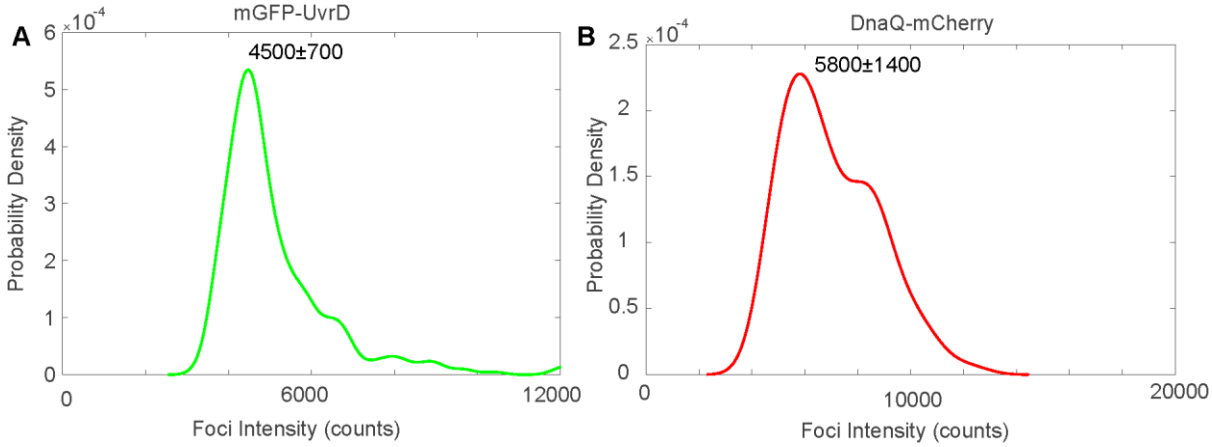

1050

1051 **Supplementary Figure S6: Brightness of single mGFP and mCherry molecules** A. and
1052 B. Characteristic intensity distributions rendered as kernel density estimates of single mGFP-
1053 UvrD and DnaQ-mCherry. Peak±full width at half maximum indicated. Distributions calculated
1054 from the tracked foci intensity distributions from the end of the photobleach process such that
1055 only single fluorophore molecules are detected. Number of molecules per foci before
1056 bleaching is determined by dividing the initial foci intensity by these values for the equivalent
1057 fluorophore.

1058

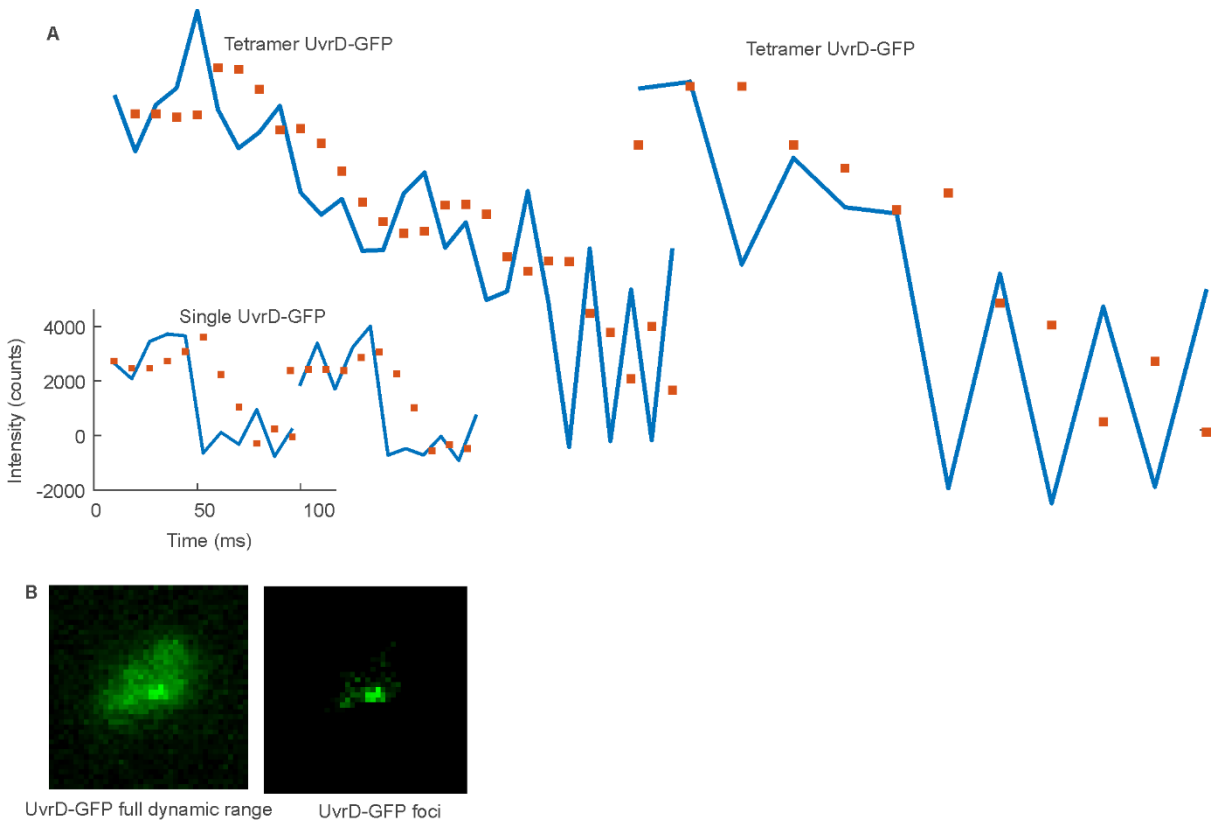

Supplementary Figure S7: Single-molecule image analysis. A. Chung-Kennedy filtered (squares) intensity traces for single UvrD tracks showing tetramers exhibiting multiple photobleach steps and monomers detected towards the end of photobleaching. Foci were 'overtracked' beyond the last detected bright frame to illustrate steps. **B**. UvrD-GFP micrograph showing the full dynamic range (left) and adjusted to illustrate a foci (right)

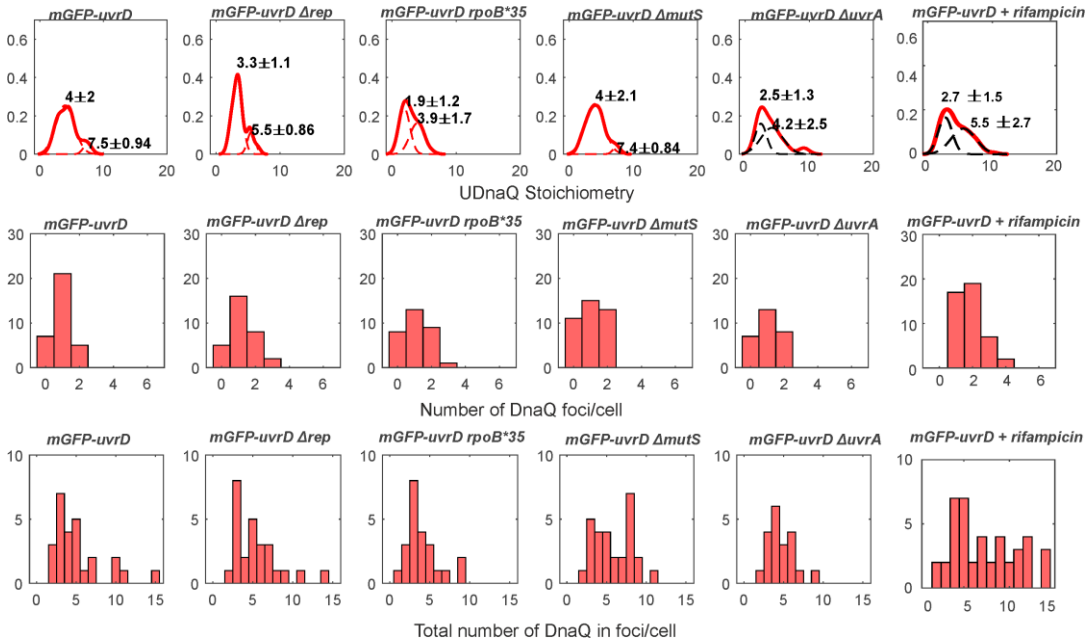

Supplementary Figure S8: DnaQ tracking characterization. Top row: Distribution of DnaQ foci stoichiometry as a kernel density estimate for all strains and conditions (red) with two Gaussian fit overlaid as black dotted lines. Peak ± half width at half maximum shown above. Middle row: Corresponding histogram of number of foci detected per cell. Bottom row: histogram of the total amount of DnaQ in foci per cell. N=30-50 cells per strain or condition.

1079

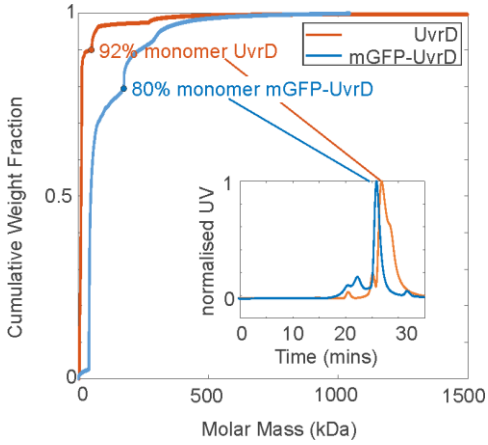

1080
1081 **Supplementary Figure S9: SEC-MALLS of UvrD/mGFP UvrD .** Size Exclusion
1082 Chromatography - Multi-Angle Laser Light Scattering (SEC-MALLS) of 4μM UvrD (red) and
1083 mGFP-UvrD (blue) cumulative weight fraction as a function of molar mass. 92% of UvrD and
1084 80% of mGFP-UvrD is consistent with a monomer. Inset shows the normalised UV
1085 abosorbance as a function of elution time through the column with the monomer peaks
1086 indicated.
1087

1088
1089

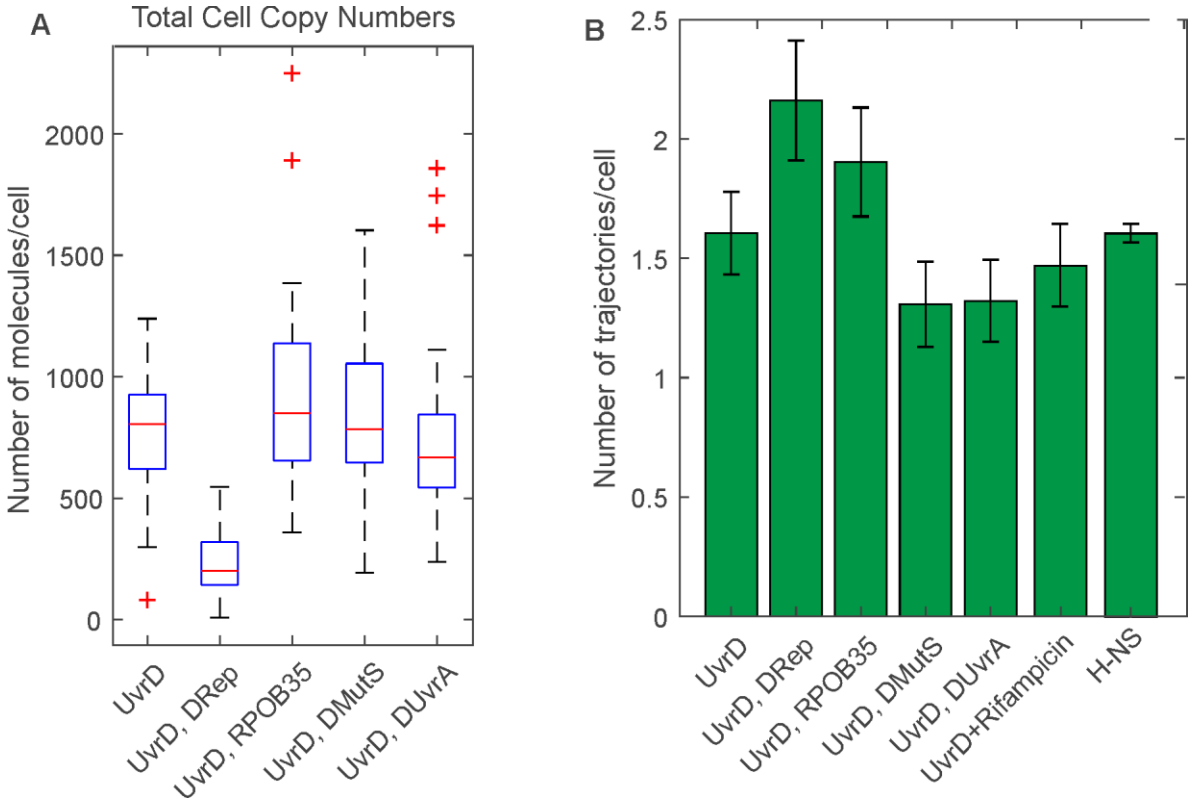

1090

1091 **Supplementary Figure S10:** A. Boxplot of the total number of mGFP-UvrD molecules per
1092 cell, estimated by numerical integration of the whole cell fluorescence. Median is shown as
1093 red line, bottom and top of the blue box mark the 25th and 75th percentiles and whiskers
1094 extend to the most extreme points not considered outliers (2.7 standard deviations covering
1095 99.3% of normally distributed data) with outliers beyond this shown as red +. N=30 cells per
1096 strain. B Number of trajectories per cell used in the stoichiometry determination
1097

1098

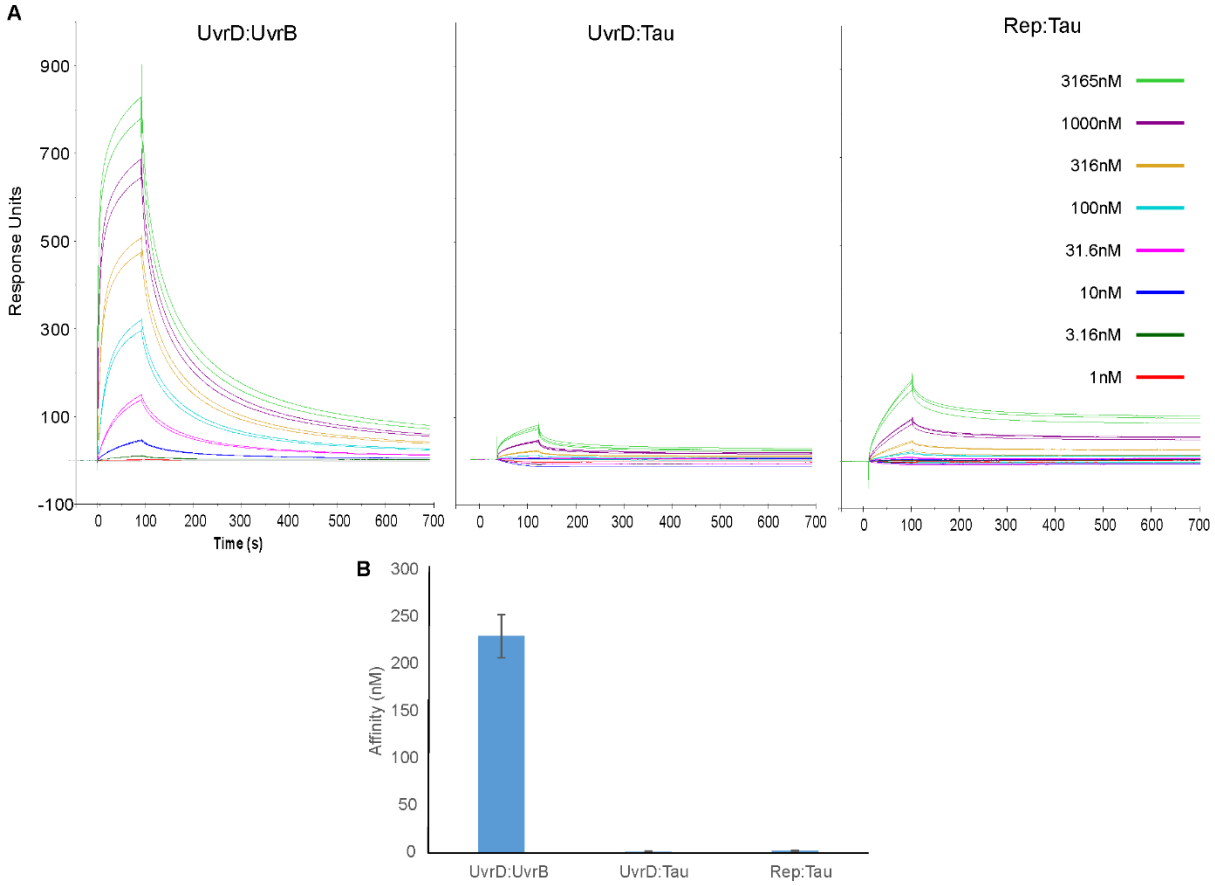

1099

1100 **Supplementary Figure S11: Surface plasmon resonance measurements of helicase**
1101 **interactions with Tau** A. Titration response curves for UvrD:UvrB, UvrD:Tau and Rep:Tau
1102 with their affinities shown in B.

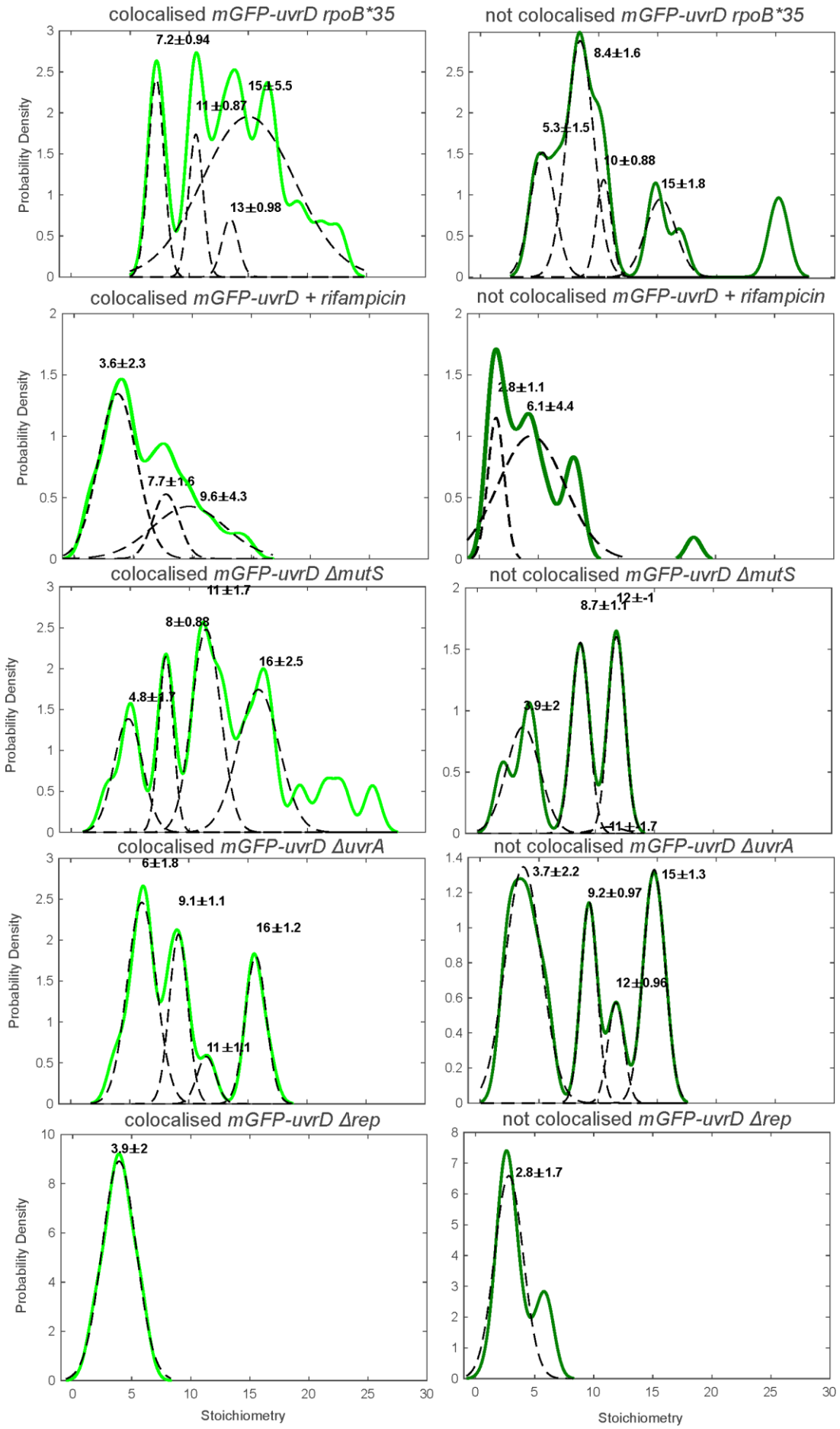
colocalised mGFP-uvrD rpoB*35
7.2±0.94
11±0.87
15±5.5
13±0.98
not colocalised mGFP-uvrD rpoB*35
8.4±1.6
5.3±1.5
10±0.88
15±1.8
colocalised mGFP-uvrD + rifampicin
3.6±2.3
7.7±1.6
9.6±4.3
not colocalised mGFP-uvrD + rifampicin
2.8±1.1
6.1±4.4
colocalised mGFP-uvrD ΔmutS
11±1.7
8±0.88
16±2.5
4.8±1.7
not colocalised mGFP-uvrD ΔmutS
8.7±1.1
12±-1
3.9±2
11±1.7
colocalised mGFP-uvrD ΔuvrA
6±1.8
9.1±1.1
16±1.2
11±1.1
not colocalised mGFP-uvrD ΔuvrA
3.7±2.2
9.2±0.97
15±1.3
12±0.96
colocalised mGFP-uvrD Δrep
3.9±2
not colocalised mGFP-uvrD Δrep
2.8±1.7
Probability Density
Stoichiometry

1103

1104 **Supplementary Figure S12:** Perturbed UvrD stoichiometry. The distribution of UvrD foci
1105 stoichiometry rendered as a kernel density estimate for foci colocalised (Left) and non-
1106 colocalised (Right) with DnaQ foci. Distributions were fitted with multiple Gaussian fits (black
1107 dotted lines) with the peak value ± half width at half maximum indicated above each peak.
1108

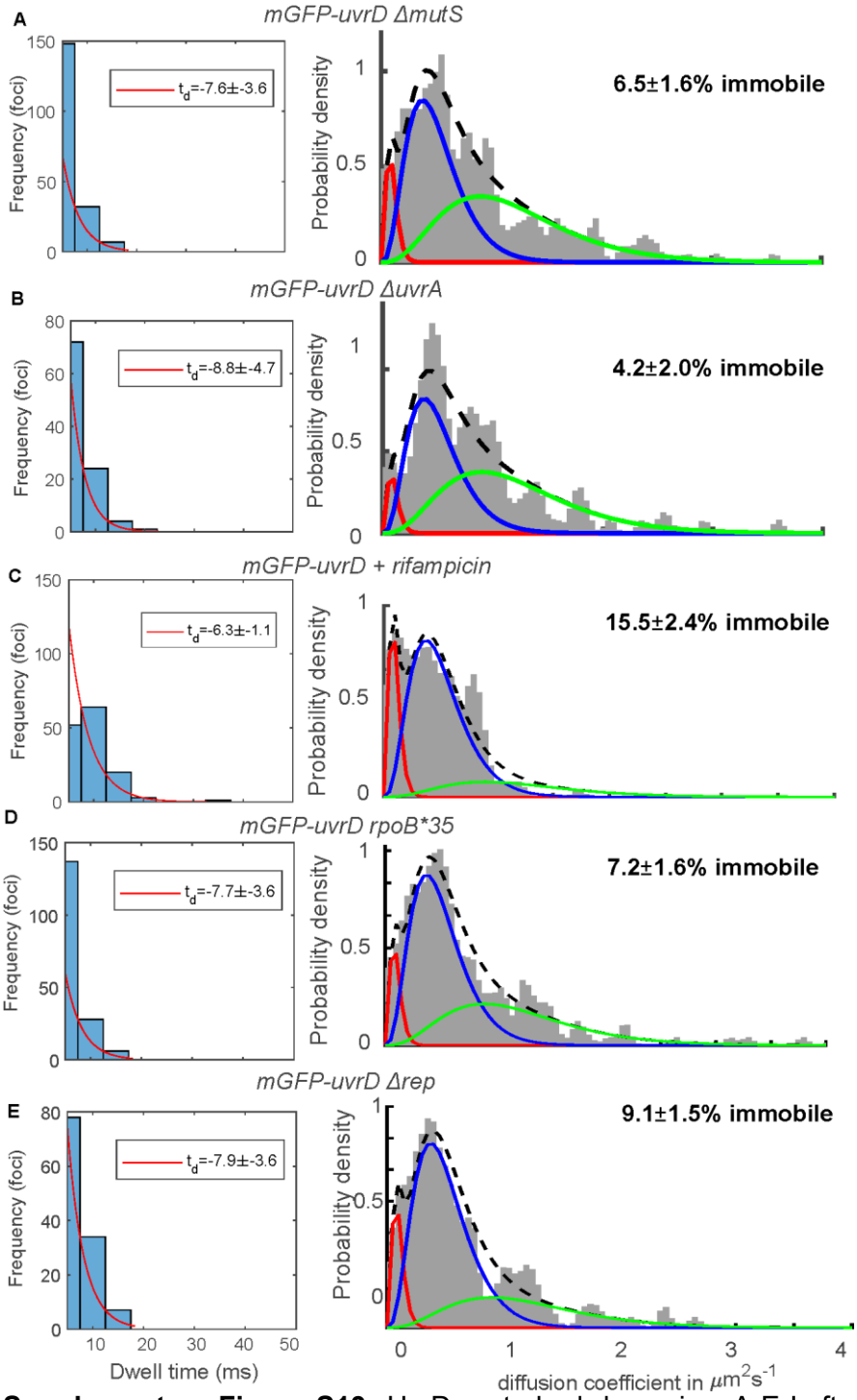

Supplementary Figure S13: UvrD perturbed dynamics. A-E Left, distribution of time UvrD and DnaQ foci were colocalised (blue) fit with an exponential (red) to yield a characteristic dwell time. Right, distribution of microscopic diffusion coefficients of UvrD foci (grey) fitted with a three state gamma distribution model containing a relatively immobile population with D = 0.1 μm^2/s (red), a transiently immobile population, D = 0.5 μm^2/s (blue) and a mobile population, D=1.2 μm^2/s (green). Errors represent 95% confidence intervals. N~300 foci/condition.

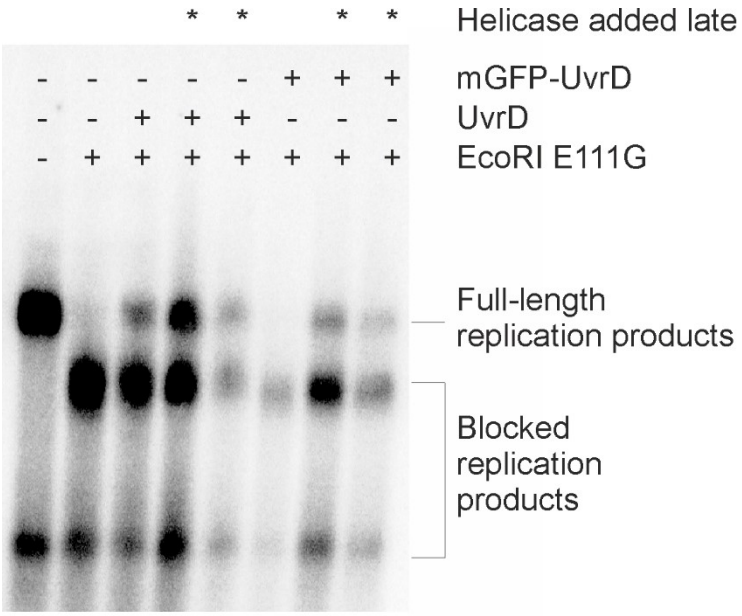

Supplementary Figure S14: In vitro replication assay using mGFP-UvrD. Denaturing agarose gel of replication products formed from pPM872 (1) in the absence and presence of EcoRI E111G block, mGFP-UvrD and UvrD added pre- and post-collision (*) as indicated.

Supplementary references

1. Baba,T., Ara,T., Hasegawa,M., Takai,Y., Okumura,Y., Baba,M., Datsenko,K.A., Tomita,M., Wanner,B.L. and Mori,H. (2006) Construction of Escherichia coli K-12 in-frame, single-gene knockout mutants: the Keio collection. *Mol. Syst. Biol.*, **2**, 2006.0008.
2. Bachmann,B.J. (1996) Derivations and genotypes of some mutant derivatives of Escherichia coli K-12. . In Neidhardt,F.C., Curtiss III,R., Ingraham,J.L., Lin,E.C.C., Low,K.B., Magasanik,B., Reznikoff,W.S., Riley,M., Schaechter,M., Umbarger,H.E. (eds), *Escherichia coli and Salmonella cellular and molecular biology*. ASM Press, Washington, DC, pp. 2460–2488.
3. Bernhardt,T.G. and de Boer,P.A.J. (2004) Screening for synthetic lethal mutants in Escherichia coli and identification of EnvC (YibP) as a periplasmic septal ring factor with murein hydrolase activity. *Mol. Microbiol.*, **52**, 1255–1269.
4. Guy,C.P., Atkinson,J., Gupta,M.K., Mahdi,A.A., Gwynn,E.J., Rudolph,C.J., Moon,P.B., van Knippenberg,I.C., Cadman,C.J., Dillingham,M.S., *et al.* (2009) Rep provides a second motor at the replisome to promote duplication of protein-bound DNA. *Mol. Cell*, **36**, 654–666.
5. Syeda,A.H., Wollman,A.J.M., Hargreaves,A.L., Howard,J.A.L., Brüning,J.-G., McGlynn,P. and Leake,M.C. (2019) Single-molecule live cell imaging of Rep reveals the dynamic interplay between an accessory replicative helicase and the replisome. *Nucleic Acids Res.*, **47**, 6287–6298.
6. Datsenko,K.A. and Wanner,B.L. (2000) One-step inactivation of chromosomal genes in *Escherichia coli* K-12 using PCR products. *Proc. Natl. Acad. Sci. USA*, **97**, 6640–6645.
7. Boubakri,H., de Septenville,A.L., Viguera,E. and Michel,B. (2010) The helicases DinG, Rep and UvrD cooperate to promote replication across transcription units in vivo. *EMBO J.*, **29**, 145–157.
8. Brüning,J.-G., Howard,J.A.L. and McGlynn,P. (2016) Use of streptavidin bound to biotinylated DNA structures as model substrates for analysis of nucleoprotein complex disruption by helicases. *Methods*, **108**, 48–55.
9. Brüning,J.-G., Howard,J.A.L., Myka,K.K., Dillingham,M.S. and McGlynn,P. (2018) The 2B subdomain of Rep helicase links translocation along DNA with protein displacement. *Nucleic Acids Res.*, **46**, 8917–8925.